Applied Geochemistry 122 (2020) 104767

Contents lists available at ScienceDirect

Applied Geochemistry

journal homepage: http://www.elsevier.com/locate/apgeochem

Depth and intensity of the sulfate-methane transition zone control sedimentary molybdenum and uranium sequestration in a eutrophic low-salinity setting

Sami A. Jokinen [a,b,c,*], Karoliina Koho [a], Joonas J. Virtasalo [c], Tom Jilbert [a,d]

[a] Aquatic Biogeochemistry Research Unit, Ecosystems and Environment Research Program, Faculty of Biological and Environmental Sciences, University of Helsinki, P.O. Box 65, FI-00014, Helsinki, Finland
[b] Lake and Marine Sediment Research Group, Department of Geography and Geology, University of Turku, FI-20014, Turku, Finland
[c] Marine Geology, Geological Survey of Finland (GTK), P.O. Box 96, FI-02151, Espoo, Finland
[d] Tvärminne Zoological Station, University of Helsinki, J.A. Palménintie 260, 10900, Hanko, Finland

ARTICLE INFO

Editorial handling by Prof. M. Kersten

Keywords:
Molybdenum
Uranium
Sulfate-methane transition zone
Eutrophication
Paleoredox
Hypoxia

ABSTRACT

Molybdenum (Mo) and uranium (U) contents in sedimentary archives are often used to reconstruct past changes in seafloor oxygenation. However, their sequestration processes are as yet poorly constrained in low-salinity coastal waters, which often suffer from anthropogenic eutrophication but only mild oxygen depletion. Due to the consequent lack of robust long-term paleo-redox reconstructions in such settings often characterized by a shallow front of dissolved sulfide accumulation within the sediment pore waters, inadequate understanding of the long-term drivers behind oxygen loss impedes cost-effective mitigation of this environmental problem. Here, we investigate the mechanisms of Mo and U sequestration in an oxic, low-salinity coastal setting in the northern Baltic Sea where anthropogenic eutrophication over the 20th century has resulted in formation of a shallow sulfate-methane transition zone (SMTZ) in the sediment column of this brackish-water basin. Our results demonstrate remarkably similar patterns for authigenic Mo and U sequestration, whereby the depth and intensity of the SMTZ exerts a first-order control on their solid-phase uptake. Sequential extraction analysis suggests that a large part of the authigenic Mo pool is hosted by refractory Fe–S phases such as pyrite and nanoscale $FeMoS_4$, implying that the Fe-sulfide pathway is the dominating process of authigenic Mo scavenging. However, we also observe a pool of extremely labile Mo deep within the SMTZ, which might record an intermediate phase in authigenic Mo sequestration and/or partial switch to the organic matter (OM) pathway at low dissolved Fe levels. Authigenic U resides in acid-extractable and refractory phases, likely reflecting uptake into poorly crystalline monomeric U(IV) and crystalline uraninite, respectively. Similarly to Mo, authigenic U uptake is active at two fronts within the SMTZ, paralleled by increases in dissolved sulfide levels, suggesting coupling between sulfide production and U reduction. Our results imply that both Mo and U could provide viable proxies for mild bottom water deoxygenation in these settings, through the indirect link between seafloor oxygen conditions and the depth of SMTZ. Of these, Mo appears to more robustly capture variations in seafloor oxygen levels due to the significantly higher share of the authigenic pool. However, temporal resolution of these proxies is limited by the vertical offset between seafloor and the zone of authigenic uptake, and the superimposed character of the signal at a given depth due to vertical migrations of the SMTZ. These results have important implications for the use of Mo and U as paleo-redox proxies in other low-salinity coastal settings exposed to eutrophication.

1. Introduction

Due to their redox-sensitive behavior, sedimentary contents of molybdenum (Mo) and uranium (U) are often used to decipher past fluctuations in seafloor oxygenation (McManus et al., 2006; Tribovillard et al., 2006; Algeo and Tribovillard, 2009; Bura-Nakić et al., 2018; van Helmond et al., 2018). Such paleo-redox reconstructions may help to delineate effective measures to mitigate coastal hypoxia, which is a

* Corresponding author. Aquatic Biogeochemistry Research Unit, Ecosystems and Environment Research Program, Faculty of Biological and Environmental Sciences, University of Helsinki, P.O. Box 65, FI-00014, Helsinki, Finland.
E-mail address: sami.jokinen@utu.fi (S.A. Jokinen).

https://doi.org/10.1016/j.apgeochem.2020.104767
Received 23 June 2020; Received in revised form 3 September 2020; Accepted 8 September 2020
Available online 14 September 2020

globally expanding environmental problem forced by excessive nutrient loading and climatic warming (Diaz and Rosenberg, 2008; Vaquer-Sunyer and Duarte, 2008; Gooday et al., 2009; Breitburg et al., 2018). Specifically, thorough understanding of the processes and associated feedback mechanisms driving deoxygenation can be gained from long-term reconstructions that encompass millennial or multi-centennial scale changes in the intensity of natural and anthropogenic forcing factors (Cooper and Brush, 1991; Jilbert and Slomp, 2013a; Erhardt et al., 2014; Moffitt et al., 2015; Jokinen et al., 2018). However, applicability of Mo- and U-based redox records is currently limited by inadequate understanding of their sequestration processes and diagenetic mobility (Bennett and Canfield, 2020). This is especially true in non-euxinic coastal settings, which are typified by diverse site-specific depositional dynamics (Algeo and Li, 2020; Algeo and Liu, 2020; Liu and Algeo, 2020). As a result, ignorance of potential caveats inherent in paleo-redox reconstructions in such environments might bias the interpretation of sediment records (e.g. Zheng et al., 2002a; McManus et al., 2005; Morford et al., 2009a; Helz et al., 2011). Crucially, along the eutrophic-hypoxic-anoxic redox continuum of human-impacted coastal systems (Diaz and Rosenberg, 2008; Breitburg et al., 2018), settings close to the eutrophic end-member are underrepresented in trace metal-based paleo-redox proxy studies.

The applicability of Mo and U as paleo-redox proxies is underpinned by their long oceanic residence times and low contents in the upper continental crust (Emerson and Huested, 1991; McLennan, 2001), enhanced particle reactivity with decreasing redox potential (Klinkhammer and Palmer, 1991; Helz et al., 1996), and negligible uptake by phytoplankton (Algeo and Tribovillard, 2009). In general, organic matter (OM) –rich sediments comprise a major oceanic sink for Mo and U, since their authigenic sequestration is driven by microbial OM remineralization reactions, which consume oxygen and other electron acceptors in the water column and at the seafloor. This indirect relationship largely explains the commonly observed coupling between authigenic sequestration of Mo and U and sedimentary organic carbon (C_{org}) content.

Mo is present in seawater as molybdate (MoO_4^{2-}), which is largely inert except for its slow adsorption onto Fe and Mn (oxyhydr)oxides (Algeo and Tribovillard, 2009). Although these solid-phases may cause transient Mo enrichments in surface sediments, the ultimate burial is triggered when dissolved hydrogen sulfide (H_2S_{aq}) levels exceed 11 μM, activating a 'geochemical switch' (Helz et al., 1996; Erickson and Helz, 2000) whereby stepwise sulfidation of MoO_4^{2-} results in the formation of a series of thiomolybdates ($MoO_{4-x}S_x$, where x = 1–4). Crucially, the $MoO_{4-x}S_x$ species exhibit increasing particle affinity with increasing degree of sulfidation (Bostick et al., 2003; Helz et al., 2004; Dahl et al., 2010), causing their effective scavenging by OM and/or Fe-sulfide phases, and hence permanent burial of authigenic Mo (Helz et al., 1996, 2011; Vorlicek et al., 2004, 2018; Freund et al., 2016; Dahl et al., 2017; Wagner et al., 2017; Helz and Vorlicek, 2019).

In euxinic settings, scavenging of Mo may operate throughout the sulfidic bottom waters, while in non-euxinic environments authigenic uptake of Mo is restricted to sulfide-rich fronts in the sediment pore waters (Scott and Lyons, 2012). Such fronts develop whenever microbial reduction of sulfate (SO_4^{2-}) produces H_2S_{aq} in excess of dissolved Fe (Rickard and Luther III, 2007), and may be located close to the sediment-water interface (SWI) or up to decimeters into the sediment column. Furthermore, SO_4^{2-} reduction may be coupled to either OM reminaralization (e.g. Jørgensen et al., 2019) or to anaerobic oxidation of methane (AOM) (e.g. Boetius et al., 2000). Authigenic Mo enrichments in non-euxinic settings are limited by the rate of MoO_4^{2-} supply to the sulfide front, often leading to orders of magnitude smaller enrichments in comparison to euxinic settings (Scott and Lyons, 2012; Helz and Adelson, 2013). Consequently, the applicability of authigenic Mo as a paleo-redox proxy in non-euxinic (e.g. seasonally hypoxic) settings is often questioned (Erickson and Helz, 2000; Helz and Adelson, 2013).

U is present in seawater predominantly as soluble U(VI) in chemically poorly reactive uranyl carbonate complexes ($UO_2(CO_3)_3^{4-}$) (Langmuir, 1978; Klinkhammer and Palmer, 1991). Analogously to Mo, solid-phase uptake of seawater U via adsorption to Fe and Mn (oxyhydr)oxides may cause transient U enrichments in oxic surface sediment environments (Brennecka et al., 2011; Dang et al., 2016). However, reducing conditions are required to initiate permanent sediment sequestration of U via reduction of U(VI) to insoluble and particle-reactive U(IV), effectively triggering its solid-phase uptake primarily through the formation of uraninite (UO_2) (Klinkhammer and Palmer, 1991; Sharp et al., 2009) and monomeric non-uraninite U(IV) (Bernier-Latmani et al., 2010; Sharp et al., 2011; Bargar et al., 2013; Bhattacharyya et al., 2017). By contrast to Mo, the sequestration of U takes place exclusively within sediments even in euxinic settings, signaling that the reduction process is enabled on solid substrates by the enzymes excreted by Fe^{3+} and SO_4^{2-} reducing bacteria (Anderson, 1987; Zheng et al., 2002b; Morford et al., 2009b; Bura-Nakić et al., 2018). The reduction of U(VI) is generally thought to occur under conditions similar to those of organo-clastic reduction of Fe^{3+} and hence above the zone of Mo sequestration (Klinkhammer and Palmer, 1991; Zheng et al., 2000; McManus et al., 2005, 2006; Chaillou et al., 2002; Morford et al., 2005, 2009a). On the other hand, several studies have demonstrated inhibition of the reduction process in the absence of bacterial SO_4^{2-} reduction (Zheng et al., 2002a,b; Sundby et al., 2004; McManus et al., 2005) or even direct coupling between these processes, whereby sulfate-reducing bacteria use U(VI) as an electron acceptor (Lovley et al., 1991, Lovley and Phillips, 1992; Bargar et al., 2013). Similarly to Mo, the relative importance of factors limiting authigenic U sequestration in non-euxinic coastal sediments, such as OM delivery, oxygen penetration depth (OPD), and the rates of Fe and SO_4^{2-} reduction, remain poorly constrained (Zheng et al., 2000; McManus et al., 2005; Morford et al., 2009a; Holmden et al., 2015), impeding its utilization as a paleo-redox proxy.

Many near-shore settings worldwide, including estuaries, lagoons, and the coastal zone of enclosed seas, are characterized by anthropogenic eutrophication of low-salinity waters (Levin et al., 2009; Fennel and Testa, 2018). These conditions generate a specific zonation of sedimentary diagenetic processes which may impact upon the sequestration of Mo and U, and hence their potential use as archives of past environmental change. Here, we aim to disentangle Mo and U sequestration mechanisms in such as system, in order to better determine the value of trace metal redox proxies in these settings. We focus on a low-salinity coastal setting in the northern Baltic Sea, where human-induced eutrophication has led to the formation of a distinct sulfate-methane transition zone (SMTZ) in the upper decimeters of the sediment column during the late 20th century. To delineate the pathways of sedimentary Mo and U uptake, we performed solid-phase sequential extraction analyses for Fe, Mn, Mo, and U (among other elements) complemented with pore water chemical analyses, from four sediment cores. Specifically, we investigate how the solid-phase speciation and pore water concentrations of Mo and U vary with respect to the general diagenetic zonation in the sediments, allowing deconvolution of the potential host phases and mechanisms for authigenic Mo and U uptake. Finally, we introduce a conceptual model for authigenic Mo and U sequestration in low-salinity, non-euxinic coastal settings characterized by high OM input and a shallow SMTZ, and discuss the applicability of these proxies for bottom water oxygenation in such environments.

2. Materials and methods

2.1. Study sites and sample collection

Storfjärden is a shallow coastal basin in the southwestern coast of Finland in the northern Baltic Sea (Fig. 1). The basin is part of the archipelago region of the Pojo Bay estuarine system. The archipelago is separated from the inner estuary by the shallow sill of the First Salpausselkä ice-marginal formation. The coastline in this area of the Gulf of Finland is typified by a mosaic of islands, capes and bays, intersected by broadly north-south trending deeper channels. This complex

topography is a manifestation of numerous glaciations that eroded the Precambrian peneplain (Winterhalter et al., 1981), whereby effectiveness of this erosion showed substantial spatial variability due to the contrasting rock types and occurrence of old fracture zones in the bedrock (Edelman, 1949).

Following its last deglaciation by 12 250 cal a BP, the study area has been subaquatic and successively covered by late- and post-glacial lacustrine clays, and brackish-water muds (Virtasalo et al., 2014). Currently, Storfjärden represents a typical middle archipelago accumulation basin where large parts of the seafloor are covered by recently deposited brackish-water mud (Virtasalo et al., 2019). Sedimentation of siliciclastic material in the area is dominated by local reworking of the previously deposited clays and muds (Virtasalo et al., 2014). Most of the sediment OM is sourced from the local primary productivity (Jilbert et al., 2018).

Salinity in the archipelago area, where Storfjärden is located, is typically 6–7 throughout the year. The water column becomes partially stratified due to summer irradiation. Respiration of authochthonous OM leads to depletion of bottom water oxygen towards the end of the stratification period (Kauppi et al., 2018), although values never cross the threshold of hypoxia (<63 μmol L^{-1} O_2). Eutrophication of the northern Baltic Sea during the late 20th century has increased the OM loading to the sediments in this system significantly (Fleming-Lehtinen et al., 2015), leading to a distinct change in the sediment diagenetic zonation. As described by Slomp et al. (2013) and Rooze et al. (2016) for the nearby Bothnian Sea, OM loading under low-salinity conditions has increased the rate of organo-clastic SO_4^{2-} reduction in the upper sediment column. This has led to a contraction of the zones of primary redox reactions and caused the SMTZ, where SO_4^{2-} reduction gives way to methanogenesis, to shoal to the uppermost decimeters of the sediment column. Very similar pore water profiles to those observed in the Bothnian Sea have been recently published for the Storfjärden area (e.g. Jilbert et al., 2018; Myllykangas et al., 2020a, here redrawn in Fig. 1C), implying a common set of processes throughout the low-salinity areas of the northern Baltic Sea. Crucially, the SMTZ dictates the position of the pore water sulfide front, through the intense production of H_2S_{aq} during SO_4^{2-}-mediated AOM (Egger et al., 2015). Hence, the SMTZ is expected to exert a strong control over Mo and U sequestration processes in this setting.

Sediment cores (core length ~20–60 cm) from Storfjärden were collected at four adjacent stations during two sampling campaigns (October 2016 and August 2017) onboard R/V *Saduria* using a GEMAX™ twin-barrel short gravity corer (Table 1; Fig. 1). At each station in October 2016, one of the duplicate cores was sliced for solid-phase analyses and the other one was sampled for pore water analyses. Stations 1, 2, and 4 were re-sampled in August 2017 for pore water

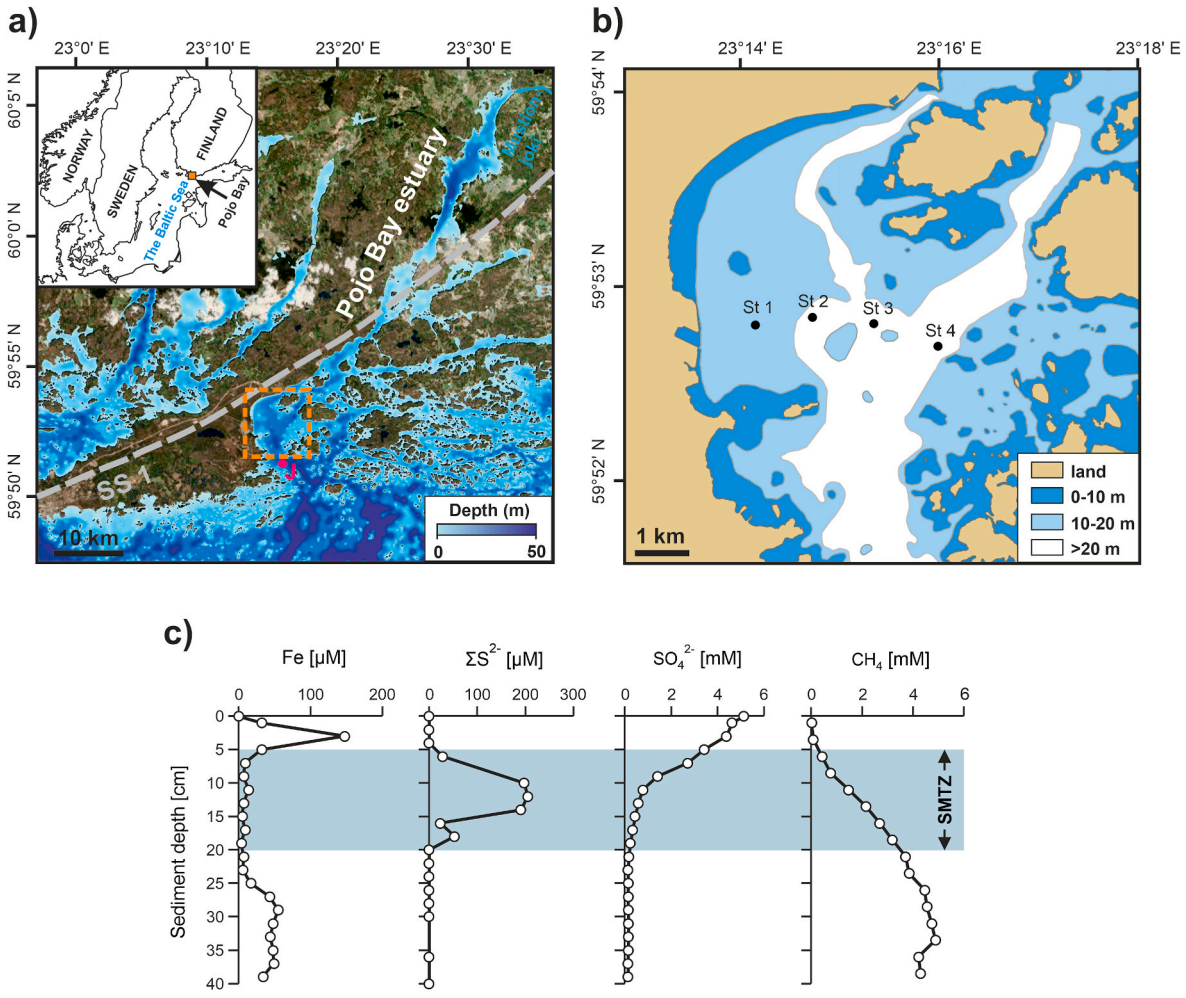

Fig. 1. **(A)** Bathymetric map of the coastal area adjacent to the Pojo Bay esturine system. SS 1 refers to the First Salpausselkä ice-marginal formation. Orange rectangle indicates the study area (Storfjärden). **(B)** Detailed bathymetric map of Storfjärden with the coring sites indicated. **(C)** Typical diagenetic zonation in the study area (data from site J in Jilbert et al. (2018), with the location indicated in panel B). Note the shallow positioning of the sulfate-methane transition zone (SMTZ), which coincides with the front of dissolved sulfide accumulation. (For interpretation of the references to colour in this figure legend, the reader is referred to the Web version of this article.)

analysis to gauge temporal fluctuations in the diagenetic processes especially in the topmost 2 dm of the sediment column. In both sampling campaigns, an additional core for oxygen profiling was retrieved from each station. In addition, prior to sediment retrieval, temperature and salinity profiles of the water column were recorded with a CTD device (Valeport MiniCTD).

2.2. Pore water analyses

2.2.1. Sampling

From each core, two parallel pore water sample series (henceforth referred to as 'bulk' and 'sulfide' series) with a vertical resolution of 2 cm were collected in polyethylene syringes through pre-drilled holes (diameter 4 mm) in the GEMAX™ core tubes using Rhizons™. In the sampling set up, the Rhizons™ were supported with a purpose-built plastic rack mounted on the core tube, and a vacuum was generated by fixing the syringe pistons open with wooden spacers. The syringes of the sulfide series were pre-filled with 1 mL of 10% zinc acetate solution to precipitate the pore water sulfide as ZnS (Jilbert et al., 2018). Subsequently, all samples were transferred from the syringes to 15 mL centrifuge tubes within 2 h of retrieval. From the bulk series samples, an aliquot was immediately taken and acidified to 1 M HNO_3 for elemental analysis by ICP-OES, and the rest was used for quantification of ammonium (NH_4^+) concentration. Finally, the core designated for dissolved oxygen analyses was subsampled from the surface with three parallel minicores (internal diameter 2.5 cm).

2.2.2. Concentration measurements

Surface sediment profiles of dissolved oxygen (O_2) were measured from each set of replicate mini-cores within 2 h of sampling at the ambient temperature with an oxygen microsensor (OX-100, Unisense) using a vertical resolution of 100 μm. Before profiling, the microsensor was two-point calibrated against filtered seawater from the study site (100% O_2 saturation) and deoxygenated solution of Na-ascorbate and NaOH (both 0.1 M, 0% O_2 saturation). Finally, measurements from the three replicate mini-cores were averaged to one stacked O_2 profile.

Pore water NH_4^+ concentration was determined spectrophotometrically from the non-acidified bulk series following methods described in Koistinen et al. (2018). The acidified subsamples from the bulk series were analyzed for elemental concentrations by ICP-MS (Thermo Fisher Scientific) at Utrecht University Department of Earth Sciences. Phosphorus (P) is assumed to be present in the pore water samples as HPO_4^{2-}, while sulfur (S) is assumed to exclusively represent SO_4^{2-}, owing to the loss of sulfide upon sample acidification (Jilbert and Slomp, 2013b). Total sulfide (ΣS^{2-}) concentration in the pore water was determined from the sulfide series samples by spectrophotometry (670 nm) after direct addition of an acidic solution of $FeCl_3$ and *N*, *N*-dimethyl-*p*-phenylenediamine (Cline, 1969; Reese et al., 2011) to sample vials. The method is based on the dissolution of the ZnS precipitate and subsequent quantitative complexation of S as methylene blue (Jilbert et al., 2018). A series of standard solutions of $Na_2S \cdot 3H_2O$ fixed in Zn acetate similarly to the samples were used to calibrate the measurements. For the calibration, the exact concentration of S in the stock solution of $Na_2S \cdot 3H_2O$ was determined by iodometric titration (Burton et al., 2008). In all of the pore water analyses, replicate measurements of samples and standards indicated analytical precision of <5%.

Table 1
Sampling locations and conducted analyses.

Station	Latitude (WGS 84)	Longitude (WGS 84)	Water depth (m)	Pore water analyses	Solid-phase analyses
St 1	59.880000	23.235917	16.5	October 2016, August 2017	October 2016
St 2	59.880667	23.245500	22.0	October 2016, August 2017	October 2016
St 3	59.880133	23.255750	22.0	October 2016	October 2016
St 4	59.878200	23.266517	23.0	October 2016, August 2017	October 2016

2.2.3. Diffusive flux calculations

Diffusive fluxes (F) of Mo and U were quantified from the pore water profiles using Fick's first law (Boudreau, 1997):

$$F = -\phi D_{sed} \frac{dC}{dx}. \quad (1)$$

where ϕ is the sediment porosity, D_{sed} is the diffusion coefficient in the sediment, and dC/dx denotes the concentration gradient in the pore water. A description of the gradient determination is given in the supplementary material (Fig. S1). The seawater diffusion coefficient (D_{SW}) for Mo was taken from Li and Gregory (1974), and following Morford et al. (2009b), we assumed that the same diffusion coefficient applies also for U. Based on the Stokes-Einstein relationship, the D_{SW} was adjusted to the ambient temperature, salinity, and pressure using an extended version of the 'diffcoeff' function (Sulu-Gambari et al., 2017) in the R package *marelac* (Soetaert et al., 2010). The pore water salinity and temperatures were assumed equal to the bottom water values obtained from the CTD cast. Finally, D_{SW} was converted to D_{sed} as follows:

$$D_{sed} = \frac{D_{SW}}{\theta^2} \quad (2)$$

For this, tortuosity (θ^2) was obtained from porosity according to Boudreau (1996):

$$\theta^2 = 1 - ln(\phi) \quad (3)$$

2.3. Solid-phase analyses

The sediment cores for solid-phase analyses were sectioned at 1 cm resolution for the topmost decimeter and at 2 cm resolution for the remaining length. The obtained sediment slices were immediately transferred into plastic bags and carefully sealed under water. Within 1 h of the sectioning, the bags were placed into a gas-tight, N_2-filled glass jar and stored at 4 °C in the dark prior to further processing. No visible signs of oxidation were observed during sectioning and storage. Subsamples of the wet sediments were later frozen, freeze-dried, and homogenized under N_2 atmosphere. Estimates for water content (weight %) and porosity (volume %) were obtained gravimetrically after freeze-drying of parallel wet samples and assuming a solid-phase density of 2.65 g cm^{-3}.

2.3.1. Carbon and nitrogen content and organic matter source determination

Subsamples of dried and ground sediments were weighed into tin capsules and measured for total C and N content by TCEA-MS at Tvärminne Zoological Station (precision and accuracy < 2.5%). Since the content of inorganic C and N is negligible in this setting (Virtasalo et al., 2005; Jilbert et al., 2018), total contents were assumed to equal to organic C (C_{org}) and N (N_{org}). The proportions of terrestrial plant-derived (%OC_{terr}) and phytoplankton-derived OM (%OC_{phyt}) were obtained from a simple two-end-member mixing model for the molar N/C ratio with end-member values of $(N/C)_{terr} = 0.04$ and $(N/C)_{phyt} = 0.13$ (Goñi et al., 2003):

$$\%OC_{terr} = \frac{(N/C)_{sample} - (N/C)_{phyt}}{(N/C)_{terr} - (N/C)_{phyt}} \times 100 \quad (4)$$

The applicability of this end-member model in similar settings has been substantiated in recent studies (Jilbert et al., 2018; Jokinen et al., 2018, 2020).

2.3.2. Total contents of Fe, Mn, S, and U

For the quantification of total solid-phase content of Fe, Mn, S, and U (among other elements), an aliquot of 0.1–0.2 g of dried and homogenized sediment was dissolved in 2.5 mL of HF (38%) and 2.5 mL mixture

of $HClO_4$ (70%) and HNO_3 (65%) (volumetric ratio 3:2) in closed Teflon bombs at 90 °C for 12 h. Following evaporation of the acids at 160 °C, the remaining gel was dissolved in Suprapur^R 1 M HNO_3 and analyzed for elemental content by ICP-MS. Based on calibration to standard solutions and checking against in-house standard sediments and replicate samples, the precision and accuracy of the analyses were <5% for all elements.

2.3.3. Sequential extraction of metals

An aliquot of 0.2–0.3 g of dried and homogenized sediment was subjected to a four-step sequential extraction procedure (Table 2) that combines aspects of the protocols of Tessier et al. (1979), Poulton and Canfield (2005), and Ruttenberg (1992). The first two stages of the extraction protocol (fractions F1 and F2) were conducted in a glove bag under anaerobic atmosphere to protect the samples from oxidation artefacts. To catalyze the reactions, the extractions were performed in centrifuge tubes that were placed into an orbital shaker (300 rpm). After each extraction step, the samples were centrifuged (2500 rpm, 5 min) and the supernatant collected for analysis either by ICP-MS (F1, F2, F4) or ICP-OES (F3). Following the stage F3, the samples were transferred to crucibles with UHQ water, taken to dryness on a hot plate and incinerated at 550 °C for 2 h. The incinerated samples were transferred back to centrifuge tubes using 1M HCl, after which the extraction procedure continued as in stages F1–F3. The residual fraction F5 was determined as a difference between total content and the sum of the fractions F1–F4. By definition, this implies that since the contents of Mo and U in F3 were generally below the detection limits of ICP-OES, some cross over from F3 to F5 might have occurred for these elements. Since any Mo or U originally present in F3 is likely associated with Fe and Mn (oxhydr)oxides (Table 2) the effects of the cross over are expected to be most pronounced in the surface sediments where these phases are most abundant (Sect. 3.2). Based on the detection limit of the ICP-OES measurements for Mo, the potential cross over comprises only a small component of F5 (generally < 20%). Analytical precision of the measurements was <5%, and reproducibility of the sequential extraction procedure was generally better than 10%. A full description of the phase distribution between the extraction steps is given in Jokinen et al. (2020).

2.3.4. ^{137}Cs analysis and linear sedimentation rate estimation

To constrain linear sedimentation rates (LSRs) for the studied cores, ^{137}Cs activity profiles for Stations 1 and 4 were obtained through measuring gamma spectra of the wet sediment samples remaining after other solid-phase analyses. The gamma spectrometric analyses were performed at the Geological Survey of Finland using a BrightSpec bMCA-USB pulse height analyzer equipped with a well-type NAI(Tl) detector. Considering that bioturbation and diffusion may cause substantial downward transport of ^{137}Cs (Holby and Evans, 1996; Klaminder et al., 2012), the sediment horizon of peak ^{137}Cs activity (instead of the initial increase) was assumed to denote radionuclide fallout emanating from the Chernobyl nuclear accident in 1986 (e.g. Ojala et al., 2017). As the target was solely to detect the relative maximum in ^{137}Cs activity, no corrections were applied to the obtained profiles (Jokinen et al., 2015, 2018). Finally, the resulting age constraints were transferred to Stations 2 and 3 through correlation of the C/N profiles (Fig. S2; Jokinen et al., 2020).

2.3.5. Calculation of excess Mo and U

To distinguish the authigenic enrichment from the lithogenic background, Mo and U contents were first normalized against Al. Subsequently, the contents of authigenic Mo (Mo_{XS}) and U (U_{XS}), were quantified following Scholz et al. (2018):

$$Me_{XS} = Me_{sample} - \frac{Me_{BG}}{Al_{BG}} \times Al_{sample} \quad (5)$$

where Me_{sample} is the measured Mo or U content, Al_{sample} is the measured Al content, and Me_{BG}/Al_{BG} represents the lithogenic background Me/Al for Mo and U. Since the authigenic sequestration of Mo and U in this setting initiates at the upper boundary of the SMTZ (Sect. 4.1.1.), we used surface-sediment Mo/Al and U/Al values at Stations 2 and 3 (not shown) as a first-order estimate for the local lithogenic background ratio. Specifically, the average of these ratios was used to approximate the Me_{BG}/Al_{BG} for both elements. Global upper continental crust Me/Al ratios (McLennan, 2001) yielded negative Mo_{XS} and U_{XS} values for the surface sediments, supporting the need for such an approach.

Mass accumulation rates (MARs) of authigenic Mo and U were calculated as follows:

$$MAR_x = C_x \times LSR \times DBD \quad (6)$$

where C_x is the content of authigenic Mo or U, LSR is the linear sedimentation rate and DBD is the dry bulk density. For this, DBD was calculated from the water content assuming solid-phase density of 2.65 g/cm^3.

3. Results

3.1. General diagenetic zonation

Oxygen penetration depth (OPD) at all stations is generally shallow (<8 mm; Fig. 2), consistent with previous studies of analogous OM-rich coastal sediments in the Baltic Sea (Hietanen and Kuparinen, 2008; Bonaglia et al., 2013). Due to the collapse of thermal stratification in late summer and reduction in phytoplankton-derived OM input towards winter, the exhaustion of dissolved oxygen in August 2017 occurs at a

Table 2
Description of the sequential extraction procedure and the main phases present in each fraction. Note that due to the wide spectrum of metal-binding ligands associated with terrestrial and phytoplankton-derived organic matter (OM), the metal-OM complexes span over fractions F2–F4. A full description of the phase distribution between different fractions is given in a parallel study (Jokinen et al., 2020).

Fraction	Operational description	Reagents	Major phases	References
F1	Exchangeable	$MgCl_2$ (1M)	Weakly-sorbed metal species	Tessier et al. (1979)
F2	Acid-soluble	Na-acetate (1M), Acetic acid, pH 4.5	Carbonates AVS Labile Me-OM complexes	Tessier et al. (1979) Cornwell and Morse (1987) Jilbert et al. (2018)
F3	Reducible	Na-dithionite (5 wt%), Acetic acid (0.35 M), Na-citrate (0.2 M), pH 4.8	Fe and Mn (oxyhydr)oxides, Labile Me-OM complexes	Poulton and Canfield (2005), Lalonde et al. (2012)
F4	Organic	Heating to 550 °C, HCl (1M)	Refractory Me-OM complexes	Ruttenberg (1992)
F5	Residual	–	Silicates Pyrite	Poulton and Canfield (2005) *Inferred*
–	Total	HF (40%), $HClO_4$:HNO_3 (3:2 vol%)		

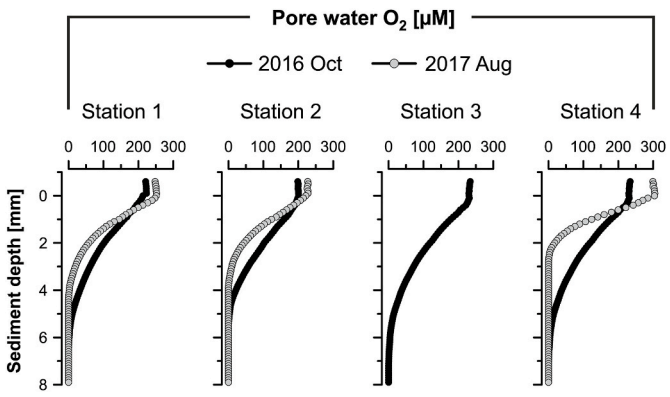

Fig. 2. Surface sediment dissolved oxygen (O_2) profiles.

shallower core depth than in October 2016, but this seasonal difference is consistently less than 3 mm.

The major pore water constituents (SO_4^{2-}, ΣS^{2-}, NH_4^+, HPO_4^{2-}, Fe and Mn) exhibit broadly similar profiles at all stations (Fig. 3), reflecting the classical diagenetic zonation of coastal sediments linked to sequential consumption of electron acceptors upon microbial OM oxidation (e.g. Froelich et al., 1979). Since a detailed description of this zonation in the sediments of the study area was recently presented by Jilbert et al. (2018), below we only briefly summarize the main features.

Due to the shallow OPD (Fig. 2), anaerobic diagenetic processes dominate the pore water chemistry. The progressive downward increases in NH_4^+ and HPO_4^{2-}, with negligible inter-annual/seasonal variation (Fig. 3), signal ongoing microbial remineralization of OM. Based on the near-surface pore water accumulation of Fe, organo-clastic reduction of Fe (oxyhydr)oxides is invariably observed at the depth of 0–10 cm irrespective of the sampling year/season. In the same zone, accumulation of Mn is occasionally observed, but this is not a consistent feature between the two sampling occasions. This interval of dissolved Fe and Mn accumulation is henceforth collectively referred to as the zone of organo-clastic reduction of Fe and Mn (OCR-Fe-Mn).

Below the zone of OCR-Fe-Mn, dissolved Fe is rapidly exhausted, simultaneously with a concave decrease in SO_4^{2-} concentration with depth, and onset of sulfide accumulation in the pore water (Fig. 3). This pattern is diagnostic for the initiation of efficient SO_4^{2-} reduction and the upper boundary of the sulfate-methane transition zone (SMTZ) at the core depth of 5–10 cm. In view of this study, it is important to note that although methane (CH_4) concentrations were not determined, a number of earlier investigations consistently show that the SMTZ in the study area coincides with the front of dissolved sulfide accumulation within the topmost decimeters of the sediment column (Fig. 1C, Jilbert et al., 2018; Myllykangas et al., 2020a, b). Building on these previous studies, we henceforth identify the upper boundary of the SMTZ based on the synchronous appearance of sulfide and depletion of Fe in the pore water profiles (Fig. 3). Within the SMTZ, the reduction of SO_4^{2-} is driven by organo-clastic sulfate reduction and oxidation of upward-diffusing methane produced deeper in the sediment in the zone of methanogenesis. Meanwhile, nutrients (NH_4^+ and HPO_4^{2-}) progressively accumulate in the pore water. The upper boundary of the SMTZ remains broadly fixed between the two sampling occasions, with the exception of Station 1. The maximum ΣS^{2-} levels reached within the SMTZ range from 300 to 500 μM. The length of the pore water profiles is generally not sufficient to constrain the lower boundary of the SMTZ, except for the year 2017 at Station 2, where it lies at a sediment depth of 12 cm, as indicated by the drawdown of ΣS^{2-}.

3.2. Profiles of the major solid-phase constituents

Solid-phase C_{org} content in the sediment is generally 4–5%. (Fig. 4). According to the N/C-based mixing model, the pool of C_{org} is dominated by phytoplankton-derived OM originating from autochthonous primary production (on average 70–85% of the total C_{org}). This component shows a downward decreasing trend at all stations, consistent with ongoing remineralization (Arndt et al., 2013). In contrast, the C/N and terrestrial C_{org} profiles are typified by a maximum in the mid-section of the cores (Figs. 4 and S2). These profiles are related to transient changes in terrestrial C_{org} input at these sites and are the focus of a parallel study (Jokinen et al., 2020), hence will not be discussed further.

Solid-phase S content ranges from 0.5 to 2.1% (Fig. 4). A general feature of the S profiles is a rapid downward increase at the transition from the zone of OCR-Fe-Mn to the SMTZ. Within the SMTZ, sedimentary S content either remains constant (Station 2) or increases towards the bottom of the cores (Stations 1, 3, and 4). Molar Fe/S ratios generally range between 2 and 6, and display an inverse relationship to S content (Fig. 4).

Based on the sequential extraction data, most of the solid-phase Fe and Mn resides in the most refractory fractions F4 and F5 (Fig. 4). However, a key feature of this data is a marked near-surface enrichment in the most labile fractions F1–F3. This enrichment is generally most pronounced at the topmost sediment sample, with the content of Fe and Mn in F1–F3 declining exponentially within the zone of OCR-Fe-Mn (Fig. 4), coinciding with the accumulation of Fe and Mn in the pore waters (Fig. 3). Overall, Fe/Al and Mn/Al ratios follow the sum of Fe and Mn in fractions F1–F3 (Fig. 4). Based on these ratios, solid-phase Mn content remains around the crustal background (McLennan, 2001) throughout the profiles, whereas Fe is consistently slightly elevated.

3.3. Mo and U profiles

A key feature of this data set is the remarkably similar behavior between Mo and U both in the dissolved and solid-phase (Fig. 5). In the near-bottom water, the concentrations of dissolved Mo and U are consistent with their expected salinity-normalized levels. Within the zone of OCR-Fe-Mn, their pore water concentrations display a generally downward decreasing trend, onto which is often superimposed a subsurface peak (Fig. 5) that coincides with dissolved Fe and Mn accumulation (Fig. 3). Within these peaks, a consistent maximum in the dissolved Mo/U ratio is observed (Fig. 5). At Stations 2 and 3, the near-surface U enrichment in F5 (Fig. 5), paralleled by Fe and Mn peaks in F3 (Fig. 4) could denote original U association with Fe and/or Mn (oxyhydr)oxides (F3) and subsequent cross over from F3 to F5 in the sequential extraction procedure (Sect. 2.3.3). Similar solid-phase surface enrichment in F5 is also observed for Mo at Station 1 (Fig. 5), but this feature is not aligned with the surface peaks of Fe and Mn in F3 (Fig. 4). Based on this offset and an upper limit for the potential cross over of Mo from F3 to F5 (based on ICP-OES detection limit, estimated to be 5 nmol g^{-1}), it is reasonable to assume that most of the enrichment genuinely resides in F5.

At the upper boundary of the SMTZ, dissolved Mo is drawn down from the pore waters, contemporaneously with a marked increase in Mo_{XS} and Mo content in F5 (Fig. 5). A similar pattern is observed for dissolved and solid-phase U, but the increase in U_{XS} is paralleled by enrichment in fractions F2 and F5. Roughly at the same depth, a general increase in solid-phase Mo/U ratio occurs. Within the SMTZ, another step-like augmentation of the Mo_{XS} and U_{XS} pools is observed. For Mo, this augmentation differs from the one observed at the upper boundary of the SMTZ in that the corresponding enrichment in the solid-phase speciation occurs not only in F5 but also in F1. For U, the speciation of this authigenic enrichment remains otherwise constant (F2 and F5), but the relative proportion of F5 is larger. At the bottom of the cores, the concentrations of dissolved Mo and U exhibit a downward increasing trend especially at Stations 1 and 4.

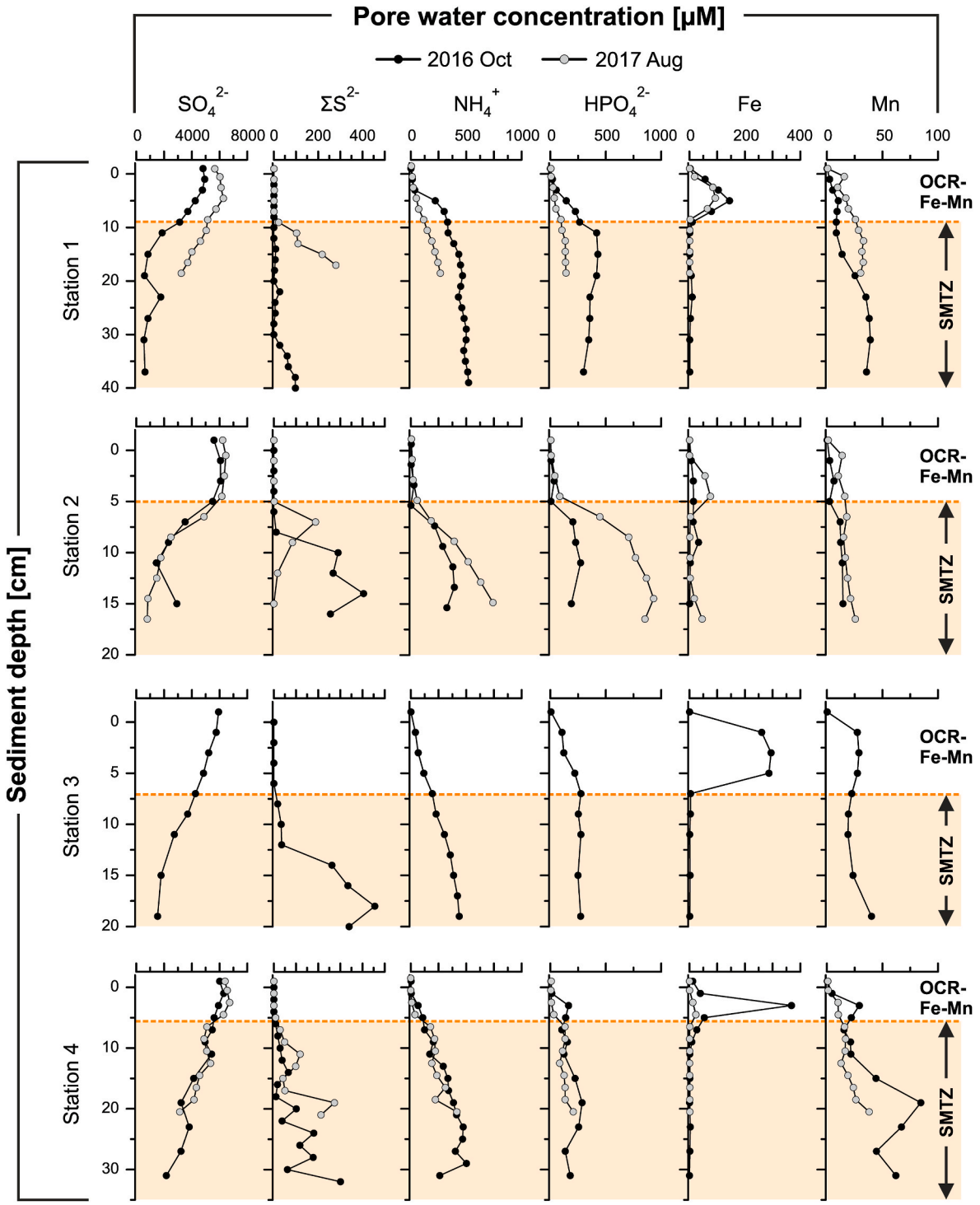

Fig. 3. Pore water profiles for the major dissolved phase constituents. Diagenetic zones of organo-clastic Fe and Mn reduction (OCR-Fe-Mn) and sulfate-methane transition (SMTZ) are also indicated. Dashed lines illustrate the shallowest position of the SMTZ upper boundary (defined based on the pore water ΣS^{2-} and Fe profiles, see the main text for details) between the two sampling occasions.

4. Discussion

4.1. Mo and U transport across the sediment-water interface

The agreement between bottom water and salinity-normalized seawater concentrations of Mo and U (Fig. 5) is compatible with their generally inert behavior under oxic conditions (Klinkhammer and Palmer, 1991; Helz et al., 1996). This implies that their potential authigenic fixation must take place either at or below the sediment-water interface (SWI), which is in line with previous studies from other non-euxinic coastal settings (Zheng et al., 2000; Adelson et al., 2001; Chaillou et al., 2002; Morford et al., 2009a,b; Helz and Adelson, 2013). Below we outline the main vectors for Mo and U transport across the SWI.

Based on the pore water profiles for Mo and U, it is apparent that both particulate shuttling (*sensu* Algeo and Tribovillard, 2009) and diffusive flux across the SWI contribute to their sequestration. Especially at Stations 2 and 3, a marked subsurface peak in dissolved Mo and U profiles is observed close to the SWI in October 2016 (Fig. 5), implying

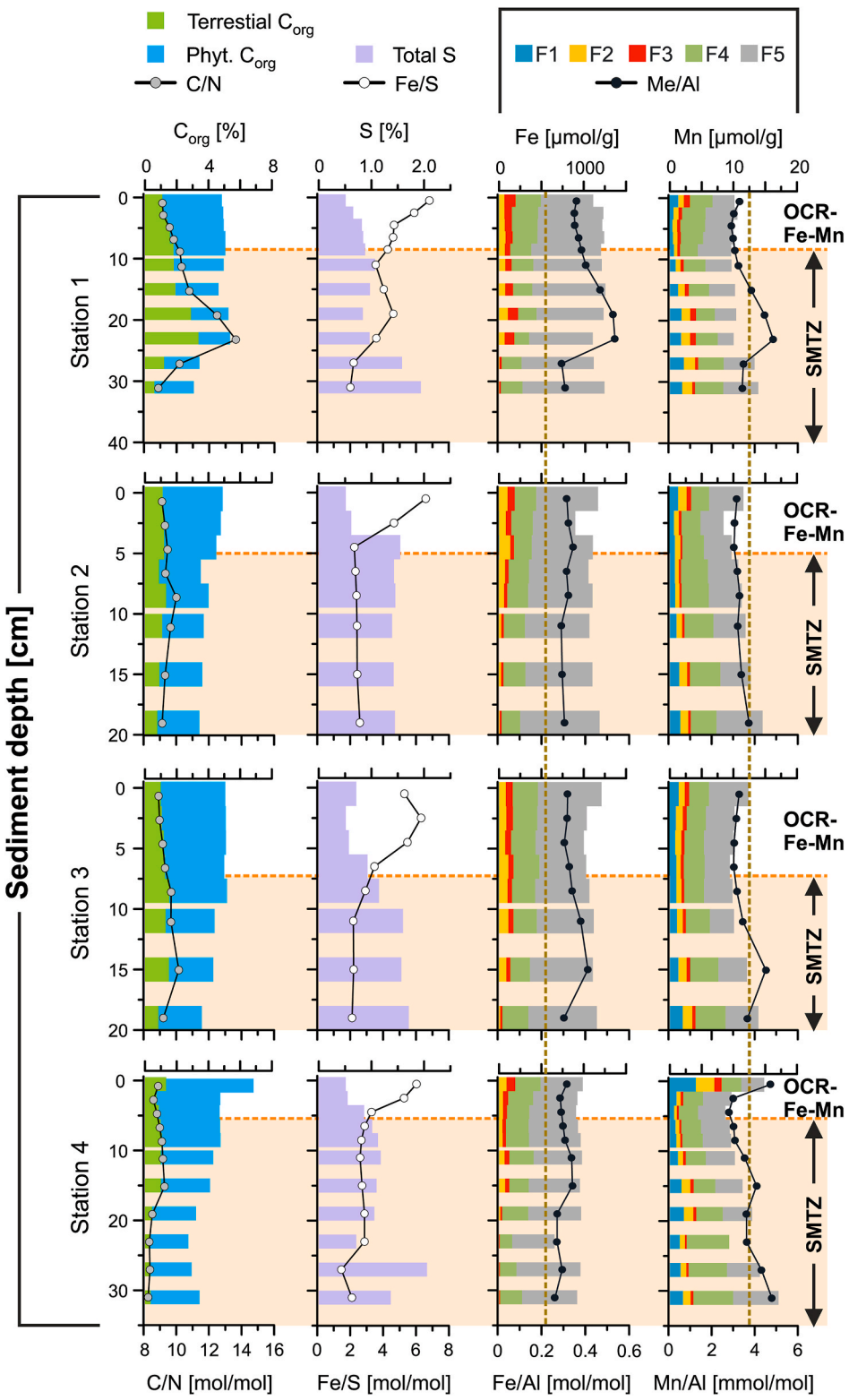

Fig. 4. Downcore profiles for the major solid-phase constituents (C_{org}, S, Fe, Mn). Organic carbon pool is divided into terrestrial plant- and phytoplankton-derived fractions based on a two-component mixing model for N/C ratio (see text for details). Molar Fe/S ratio is shown together with total S content. Solid-phase pools of Fe and Mn are divided into five different fractions (F1–F5) based on a sequential extraction scheme (Table 2). Fe/Al and Mn/Al profiles are presented alongside the sequential extraction data, with upper continental crust-based background ratios indicated (vertical dashed lines, McLennan, 2001). Diagenetic zonation as in Fig. 3.

that dissolution from a particulate phase is accentuating the flux of these elements towards the SMTZ. The dissolution front generally occurs directly below the solid-phase surface enrichment of Fe and Mn in the most labile fractions F1, F2, and F3 (Fig. 4), and broadly coincides with the peaks in pore water concentration of these elements in the zone of OCR-Fe-Mn (Fig. 3). This pattern indicates an active vertical particulate shuttle, whereby recycling of reactive Fe and Mn across the SWI deliver dissolved Mo and U to sediment pore waters (e.g. Scholz et al., 2017). The reactive forms of Fe and Mn in F1, F2, and F3 include metal-OM complexes and (oxyhydr)oxides (Jokinen et al., 2020) each of which may participate in microbial OM degradation processes.

The particulate shuttling appears to preferentially elevate dissolved Mo concentrations in comparison to U, as illustrated by the corresponding peak in dissolved Mo/U ratio (Fig. 5). This is underpinned by previous findings that emphasize the role of particulate shuttling, especially by Mn and Fe cycling, as a supplier of dissolved Mo in

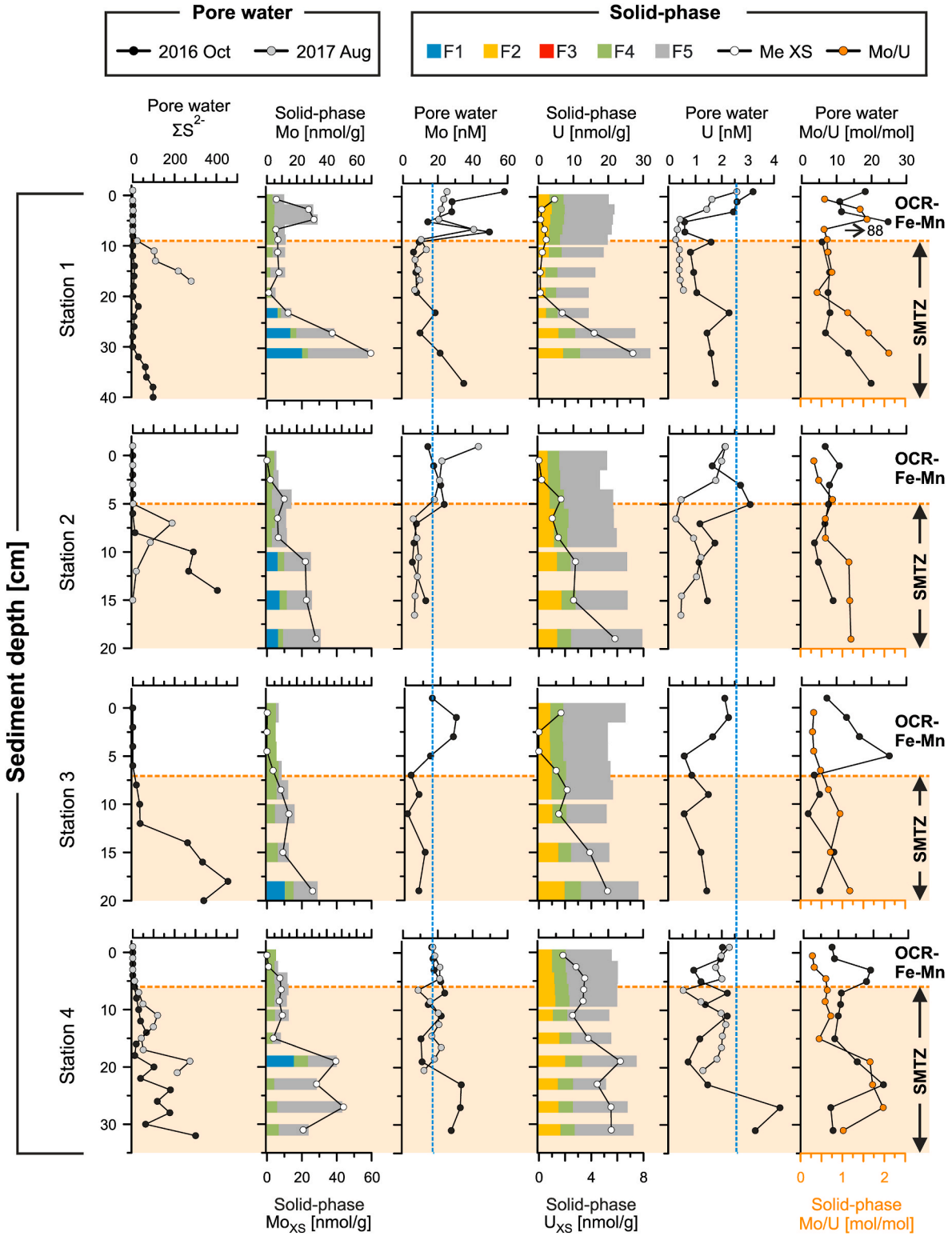

Fig. 5. Pore water ΣS^{2-} profiles alongside dissolved and solid-phase profiles for Mo and U. Solid-phase pools of Mo and U are divided into five different fractions (F1–F5) based on a sequential extraction scheme (Table 2). Contents of authigenic Mo (Mo_{XS}) and U (U_{XS}) are shown superimposed on the solid-phase Mo and U profiles, respectively. Dissolved and solid-phase Mo/U ratios are also presented. Dashed blue lines denote salinity-normalized concentrations of dissolved Mo (Nägler et al., 2011) and U (Löfvendahl, 1987) in the Baltic Sea water. Diagenetic zonation as in Fig. 3. (For interpretation of the references to colour in this figure legend, the reader is referred to the Web version of this article.)

sediment pore waters (Chaillou et al., 2002; Morford et al., 2005, 2007; Scheiderich et al., 2010; Scott and Lyons, 2012; Scholz et al., 2013, 2018; Noordmann et al., 2015; Sulu-Gambari et al., 2017), whereas the delivery of dissolved U is more often ascribed to diffusive influx from the bottom water (Anderson, 1987; Klinkhammer and Palmer, 1991; Chaillou et al., 2002; McManus et al., 2005; Algeo and Tribovillard, 2009; Morford et al., 2009a; Scholz et al., 2013; Bura-Nakić et al., 2018).

4.2. Mechanisms of authigenic Mo sequestration

A general feature of the Mo profiles in the studied cores is pore water depletion concurrently with an increase in Mo_{XS} at the upper boundary of the SMTZ (Fig. 5). Within the SMTZ, dissolved Mo displays the asymptotic profiles typical of authigenic sequestration (Zheng et al., 2000; Morford et al., 2005, 2007). The results conform to the commonly held theory that the uptake of Mo is triggered by the conversion of conservative molybdate (MoO_4^{2-}) ions to particle-reactive thio-molybdates ($MoO_{4-x}S_x^{2-}$) when [H_2S_{aq}] exceeds 11 μM (Helz et al., 1996; Erickson and Helz, 2000). Assuming a bottom water salinity of 5.8, temperature of 7.6 °C (averages from the CTD casts), and pH of 6.6 (Virtasalo et al., 2005), activation of this 'geochemical switch' should occur at ΣS^{2-} concentration of ~15 μM (calculated with R package *AquaEnv*, Hoffmann et al., 2010). Hence, at the prevailing low pore water pH, where dissolved sulfide mainly occurs in the form of H_2S_{aq}, effective Mo scavenging is enabled already at relatively low ΣS^{2-} levels. In addition to the authigenic uptake of Mo at the upper boundary of the SMTZ, the solid-phase profiles at each station consistently indicate another specific front of their authigenic sequestration deeper within the SMTZ. This front generally coincides with a steep increase in [ΣS^{2-}] to > 100–200 μM (Fig. 5), corresponding to [H_2S_{aq}] of 70–150 μM. Similar two-threshold patterns of authigenic Mo sequestration have been observed within sulfidic pore waters of other non-euxinic settings (Zheng et al., 2000; McManus et al., 2006). In the following, we discuss the most likely mechanisms of Mo enrichment at each of the two fronts in the context of the two main pathways suggested for authigenic Mo sequestration in sediments: (1) the Fe sulfide pathway (Helz et al., 1996, 2011; Freund et al., 2016) and (2) the OM pathway (Wagner et al., 2017; Dahl et al., 2017).

A cross-plot between Mo_{XS} and the sum of Mo in fractions F1 and F5 (Fig. 6A) suggest that authigenic Mo almost exclusively resides in these fractions. Hence, based on the lack of Mo in F1 at the upper front of Mo uptake where low ΣS^{2-} levels prevail, we infer that the Mo sequestered within this zone is predominantly hosted in F5. Because this residual fraction is not expected to include OM (Table 2, Jokinen et al., 2020), we further conclude that authigenic Mo sequestration at this front is likely proceeds through the Fe sulfide pathway. Along this pathway, candidate host phases for authigenic Mo in F5 include pyrite (Huerta-Diaz and Morse, 1992; Bostick et al., 2003; Vorlicek et al., 2004; Sundby et al., 2004; Tribovillard et al., 2008; Morgan et al., 2012) and discrete nanoscale Fe–Mo–S phases such as $FeMoS_4$ (Helz et al., 2011; Vorlicek et al., 2018; Helz and Vorlicek, 2019). Considering the broadly similar reactivity of Mo hosted in pyrite and in colloidal $FeMoS_4$, and that the disulfide ligands in $FeMoS_4$ precipitates might attach on pyrite surfaces (Vorlicek et al., 2018), our sequential extraction data does not allow us to constrain the relative importance between these two potential host phases.

Irrespective of the exact coordination environment of Mo sequestered at the upper boundary of the SMTZ, we infer that the solid-phase uptake of Mo through the Fe sulfide pathway at relatively low and seasonally variable ΣS^{2-} levels is stimulated by two specific factors. Firstly, locally elevated sulfide concentrations likely prevail within OM-rich microenvironments, wherein the rate of organo-clastic SO_4^{2-}

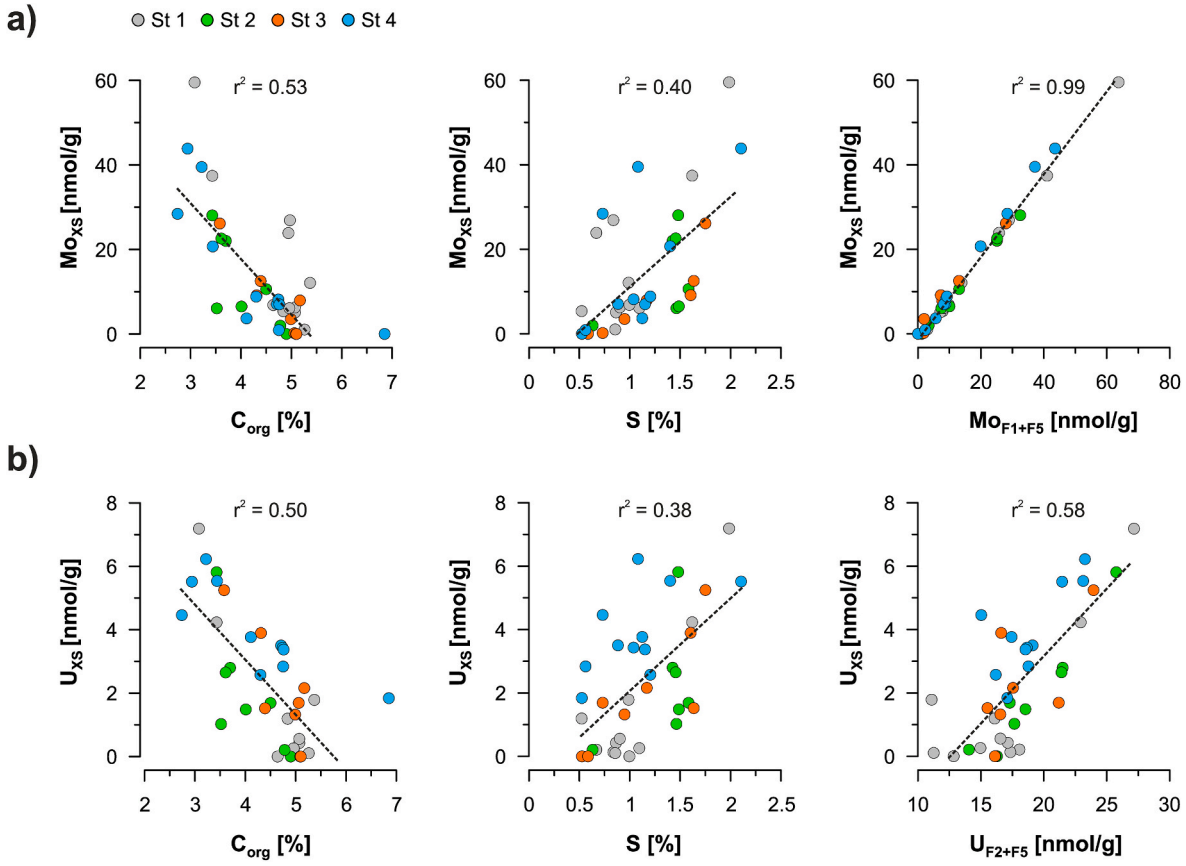

Fig. 6. **(A)** Cross-plots for authigenic Mo versus C_{org}, total S, and the sum of Mo in fractions F1 and F5. **(B)** Cross-plots for authigenic U versus C_{org}, total S, and the sum of U in fractions F2 and F5.

reduction is high (e.g. Widerlund et al., 2012). Such microniches have been proposed to act as hot spots for authigenic Mo uptake in sedimentary environments characterized by low bulk pore water ΣS^{2-} levels (Zheng et al., 2000; Helz et al., 2004). In addition, solid-phase sequestration of Mo at this front is likely stimulated by seasonal fluctuations in the vertical position of the diagenetic zonation (Fig. 3), which augments S^0 production at the upper boundary of the SMTZ (e.g. Rozan et al., 2000; Dahl et al., 2013). This zero-valent S, in turn, enhances authigenic Mo uptake via ligand-induced reduction of thiomolybdate Mo from the oxidation state of VI to IV, which is thought to trigger effective Mo scavenging from solution into Fe sulfides (Vorlicek et al., 2004; Dahl et al., 2013; Freund et al., 2016). Further in this vein, conditions favorable for Mo sequestration through this mechanism should also be conducive for efficient pyrite formation (Vorlicek et al., 2004; Rickard and Morse, 2005; Rickard and Luther, 2007), which concurs with the coincident downward increase in solid-phase S content and a decline in Fe/S ratio at the upper boundary of the SMTZ (Fig. 4), suggesting pyrite formation.

The occurrence of another, deeper front of authigenic Mo sequestration at higher ΣS^{2-} levels could denote the depth where $[H_2S_{aq}]$ permanently exceeds 11 μM (Fig. 5). While Mo fixation at the upper boundary of the SMTZ is plausibly kinetically limited by incomplete conversion of MoO_4^{2-} to MoS_4^{2-} resulting from seasonal fluctuations in $[H_2S_{aq}]$ (Erickson and Helz, 2000; Dahl et al., 2010), the permanently high sulfide levels deeper within the SMTZ promote establishment of a thermodynamic equilibrium in the dissolved Mo pool. The implication of this difference is that in the deeper front of authigenic Mo sequestration, dissolved Mo is almost exclusively in the form of MoS_4^{2-}, which exhibits substantially stronger particle-affinity than oxythiomolybdates, leading to efficient Mo burial within this zone (Bostick et al., 2003; Helz et al., 2004; Dahl et al., 2010).

In contrast to the upper front of authigenic Mo sequestration, a substantial component of solid-phase Mo uptake at the deeper front resides in the extremely labile fraction F1 in addition to F5 (Fig. 5). This observation is novel and potentially critical in understanding the mechanisms of authigenic Mo uptake and burial. Based on the extremely labile character of F1, we infer that the host phases for Mo in this fraction comprise metastable/labile phases along the Fe sulfide and/or OM pathways, potentially recording an intermediate step in authigenic Mo sequestration. The enhanced particle affinity of $MoO_{4-x}S_x^{2-}$ species with increasing degree of sulfidization (Bostick et al., 2003; Helz et al., 2004; Xu et al., 2006; Dahl et al., 2010) would imply that less sulfidized, weakly-sorbed intermediate thiomolybdates are plausible candidate phases. However, we note that this interpretation contrasts with the predominance of MoS_4^{2-} in the dissolved Mo pool at the prevailing high ΣS^{2-} in this zone. Alternatively, if low dissolved Fe levels in the SMTZ (Fig. 3) suppress Mo scavenging via the Fe sulfide pathway as suggested in previous studies (Zheng et al., 2000; Helz et al., 2011; Vorlicek et al., 2018), formation of organic thiomolybdates upon thiolation of OM is a possible interpretation (Adelson et al., 2001; Tribovillard et al., 2004; Freund et al., 2016; Wagner et al., 2017).

A further alternative explanation for the occurrence of Mo in F1 is the potential redistribution of trace metals upon sample pretreatment by freeze-drying (e.g. Kersten and Förstner, 1986; Bordas and Bourg, 1998; Hjorth, 2004) from the refractory fractions towards more labile phases. For example, Huang et al. (2015) demonstrated that oxidation of sediment samples during the drying process may redistribute As, which forms oxyanions similarly to Mo, from refractory sulfides and OM to non-specifically sorbed labile phases. Yet, despite the order of magnitude higher total As contents in comparison to Mo, we observed no As in F1 in our samples (Jokinen et al., 2020), indicating negligible redistribution to this fraction. Furthermore, the lack of Mo in F1 within some of the intervals of substantial Mo uptake into F5 (Fig. 5; e.g. Station 4, 22–32 cm sediment depth) suggests decoupling between Mo in F1 and authigenic sequestration in F5, and that the former is not sourced from oxidation of the latter. Taken together, we infer that oxidative redistribution from refractory phases is not a likely source for Mo in F1.

The increased importance of Mo scavenging by OM in comparison to Fe sulfides deeper within the SMTZ is corroborated by the findings of Tribovillard et al. (2004) who demonstrated enhanced Mo uptake by sulfidized OM in settings typified by a surplus of dissolved sulfide with respect to reactive Fe. This partial switch in the mode of authigenic Mo sequestration in favor of the OM pathway could be assisted by the downward increase in the number of reactive functional groups in DOM with progressive OM degradation, which catalyzes OM complexation to Mo (Wagner et al., 2017). However, we note that authigenic Mo sequestration may simultaneously proceed through both the Fe sulfide and the OM pathways, as suggested by the uptake of Mo into two contrasting fractions (F1 and F5) at this deeper front.

Considering both of the sequestration fronts together, we infer that authigenic Mo uptake in the studied sediments predominantly proceeds through the Fe sulfide pathway, as suggested by the coupling between Mo_{XS} and solid-phase S (Fig. 6A), which serves a first-order proxy for pyrite content in Pojo Bay sediments (Jilbert et al., 2018). This assertion in line with the growing body of evidence that the Fe sulfide pathway largely controls sedimentary Mo sequestration in organic-rich sediments (Vorlicek et al., 2018; Helz and Vorlicek, 2019). Accordingly, in contrast to the suggested intimate association between Mo sequestration and sedimentary OM (Algeo and Lyons, 2006; Lyons et al., 2009; Dahl et al., 2017; Wagner et al., 2017), these parameters are decoupled in our data (Fig. 6A).

4.3. Mechanisms of authigenic U sequestration

Similarly to Mo, the consistent drawdown of pore water U contemporaneously with an increase in U_{XS} clearly signals initiation of authigenic sequestration at the upper boundary of the SMTZ (Fig. 5). This contrasts with the general view that the onset of authigenic U sequestration occurs at shallower depth in the sediment than that of Mo (e.g. Morford et al., 2009a) due to the microbially-mediated coupling between U(VI) reduction to U(IV) and reductive Fe dissolution (Klinkhammer and Palmer, 1991; Chaillou et al., 2002; Morford et al., 2005; Scholz and Neumann, 2007; Morford et al., 2009a). Our results therefore favor the alternative interpretation that the reduction of U is linked to SO_4^{2-} reduction instead (Lovley et al., 1991, Lovley and Phillips, 1992; Hyun et al., 2012; Bargar et al., 2013; Gallegos et al., 2013; Lee et al., 2013; Bone et al., 2017).

Analogously to Mo, the U_{XS} profiles point to intensified authigenic sequestration of U deep within the SMTZ, where permanently high ΣS^{2-} levels are sustained (Fig. 5), further suggesting coupling between SO_4^{2-} reduction and U immobilization. Sulfate-reducing bacteria may use U (VI) as an electron acceptor (Lovley et al., 1991, Lovley and Phillips, 1992; Bargar et al., 2013; Zhou et al., 2014; Stylo et al., 2015), and several studies have highlighted that Fe sulfides may participate in the reduction of U(VI) (Wersin et al., 1994; Scott et al., 2007; Descostes et al., 2010; Hyun et al., 2012; Bargar et al., 2013; Gallegos et al., 2013; Lee et al., 2013; Bone et al., 2017). In addition, it has been demonstrated that U(VI) reduction may be coupled to sulfide oxidation in anoxic aqueous systems with a low carbonate content (Hua et al., 2006; Zhou et al., 2014; Stylo et al., 2015), compatible with the conditions within the SMTZ of this study. Finally, both experimental work (Zhou et al., 2014) and field-based investigations (Wang et al., 2014) suggest that the removal efficiency of U is effectively controlled by the relative abundances of dissolved Fe^{2+} and S^{2-}, whereby an excess of sulfide promotes U immobilization. These studies collectively demonstrate coupling between sulfide-generating processes and authigenic U uptake, potentially explaining the observed U sequestration deep within the SMTZ (Fig. 5) where sulfide abounds.

The sequential extraction data suggests that authigenic U predominantly resides in fractions F2 and F5. This is evidenced by the concurrent increases in U_{XS} and U content in F2 and F5 (Fig. 5) alongside with the overall strong coupling between U_{XS} and U_{F2+F5} (Fig. 6B). Furthermore,

as opposed to Mo, we observe no marked changes in authigenic U speciation with depth (Fig. 5). With respect to the F5, we postulate that the most plausible host phase for authigenic U uptake in this fraction is crystalline uranite. This contention is based on the relatively refractory character of crystalline uraninite especially under reducing conditions with low carbonate concentration (Senko et al., 2007; Ulrich et al., 2008; Sharp et al., 2011; Cerrato et al., 2013) and its generally accepted role in the sequestration of authigenic U (Klinkhammer and Palmer, 1991). Noteworthy is also that Fu et al. (2018) observed dissolution of uraninite in the Fe–Mn oxide fraction (extracted with hydroxylamine) of their sequential extraction procedure. This implies that, since we were not able to measure U in F3, at least a part of the authigenic U in our F5 might in fact dissolve already in F3 (cross over effect). Furthermore, in addition to uraninite, part of the U sequestered in F5 could be associated with pyrite (Wersin et al., 1994; Scott et al., 2007; Descostes et al., 2010), as suggested by the coupling between solid-phase S content and U_{XS} (Fig. 6B).

In contrast to F5, more labile host phases must be invoked to explain the presence of authigenic U in F2. Indeed, recent studies on U biogeochemistry emphasize the role of 'monomeric' non-uraninite U(IV) in authigenic U sequestration (Bernier-Latmani et al., 2010; Sharp et al., 2011; Boyanov et al., 2011; Bargar et al., 2013; Newsome et al., 2015; Stylo et al., 2015; Bhattacharyya et al., 2017; Bone et al., 2017). This non-crystalline U(IV) is fixed in the sediment primarily through complexation with OM (Bernier-Latmani et al., 2010; Bargar et al., 2013; Bhattacharyya et al., 2017 Bone et al., 2017) and exhibits greater lability than uraninite due to the lack of direct bonding between U atoms (hence the term 'monomeric') (Sharp et al., 2011; Alessi et al., 2012, 2014; Cerrato et al., 2013; Stylo et al., 2015). These findings are compatible with the occurrence of authigenic U in F2, and, indeed, Fu et al. (2018) found that monomeric U(IV) dissolved in the carbonate fraction (extracted with NH_4OAc in 2 M HOAc) of their sequential extraction scheme. Further support for the contribution of monomeric U (IV) in F2 is provided by the suggested inhibition of uraninite precipitation in the presence of phosphate (Bernier-Latmani et al., 2010; Boyanov et al., 2011; Veeramani et al., 2011), which is observed in high concentrations within the SMTZ at our study sites (Fig. 3). Taken together, we conclude that the observed occurrence of two different pools of authigenic U (F2 and F5) supports the previous assertions that U (IV) in OM-rich sediments is principally a mixture of monomeric U(IV) and uraninite (Sharp et al., 2011; Alessi et al., 2012; Bargar et al., 2013).

4.4. Relative efficiencies of authigenic Mo and U sequestration and the balance between diffusive fluxes and mass accumulation rates

Depth variations in dissolved and solid phase Mo/U ratios allow us to compare the relative efficiencies of authigenic sequestration of Mo and U (Fig. 5). A general feature of Mo/U profiles is a shift to lower dissolved Mo/U paralleled by an increase in solid-phase Mo/U at the upper boundary of the SMTZ. This inverse pattern between Mo/U ratios for solid and dissolved phase with sediment depth clearly illustrates the non-linear response of Mo sequestration upon the activation of the 'geochemical switch' (Helz et al., 1996). Overall, the authigenic sequestration in the solid-phase is substantially more pronounced for Mo than for U at our study sites, contrasting with the general paradigm that U is more effectively incorporated in sediments in non-euxinic settings where sulfide is restricted to pore waters (Algeo and Tribovillard, 2009). However, this observation is in line with studies from continental margin settings, where it has been observed that the efficiency of authigenic Mo sequestration increases with respect to U as pore water oxygen concentrations decrease and sulfide levels increase (McManus et al., 2006; Morford et al., 2009a).

In order to determine whether the studied sediments are at a steady-state with respect to Mo and U sequestration rates, we compared the downward diffusive fluxes of these elements in the pore waters with average authigenic mass accumulation rates (MARs of Mo_{XS} and U_{XS}) within the SMTZ (Table 3, see also Fig. S1). These estimates suggest that the downward diffusive fluxes of Mo and U from the zone of OCR-Fe-Mn towards the SMTZ are generally slightly lower than the average MARs of Mo_{XS} and U_{XS} within this zone, although of a similar order of magnitude. Specifically at Stations 2 and 3, there is a remarkable balance in the Mo and U budgets, suggesting at least quasi-steady-state conditions, whereas at Station 4 the authigenic sequestration rates of Mo and U more substantially exceed the downwards diffusive fluxes.

The imbalances in some of the Mo and U budgets imply that an additional source of dissolved Mo and U needs to be invoked to explain the observed rates of sequestration in the SMTZ. We suggest that the mismatches are at least partly attributed to upward diffusion from a deep-sourced supply, which is supported by the increasing pore water Mo and U at the bottom of the cores (Fig. 5). Indeed, the corresponding diffusive flux calculations suggest that a deep source may account for a substantial portion of the authigenic Mo and U sequestration within the SMTZ (Table 3). This deep generation of dissolved Mo and U is plausibly linked to anaerobic oxidation of methane (AOM) by Fe–Mn (oxyhydr) oxides (Beal et al., 2009; Egger et al., 2015), which is an active process below the SMTZ in Pojo Bay sediments (Myllykangas et al., 2020b). In addition to the deep-sourced supply, the mismatches in Mo and U mass balances could reflect uncaptured seasonal changes in their supply from above the SMTZ, possibly ascribed to Mn refluxing (Adelson et al., 2001; Sulu-Gambari et al., 2017). Finally, we note that the negative mass balances could also be partly attributed to the effects of bioturbation and bioirrigation (Morford et al., 2009a), which are ignored in our diffusive flux calculations.

4.5. Implications for utilizing Mo and U as paleo-redox proxies

4.5.1. The limiting factor for authigenic Mo and U sequestration

The authigenic sequestration of Mo and U observed at our study locations supports the potential of these elements to track changes in bottom water oxygenation in non-euxinic settings. Although the amplitude of authigenic enrichment is relatively modest for both elements, we suggest that the rate of their solid-phase uptake is strongly dependent upon the vertical positioning of the SMTZ in such settings (Fig. 7), since this largely dictates the diffusive flux of dissolved Mo and U to the zone of their authigenic sequestration.

With respect to Mo, our findings are in line with previous studies that highlight the importance of pore water sulfide fronts in dictating the rate of authigenic sequestration in eutrophic but generally non-euxinic coastal settings (Zheng et al., 2000; Adelson et al., 2001; Sundby et al., 2004; Helz and Adelson, 2013; Jokinen et al., 2018). The largely analogous behavior of U strongly suggests that these same factors are limiting its solid-phase uptake within the sediment. This first-order control of SMTZ characteristics over U uptake adds to the list of previously suggested limiting factors for authigenic U sequestration including OPD, delivery of OM, and the rates of organo-clastic reduction of Fe and SO_4^{2-} (Klinkhammer and Palmer, 1991; McManus et al., 2005; Morford et al., 2009a,b).

The overriding control of the depth and intensity of SMTZ on Mo and U sequestration implies that their authigenic uptake is not merely a function of OM delivery, but it more accurately mirrors the balance between the inputs of labile OM and electron acceptors at the seafloor (Middelburg and Levin, 2009). This suggests that authigenic sequestration of Mo and U is augmented when the balance shifts in favor of labile OM, which leads to shoaling of the SMTZ in the sediment column. In such conditions, bottom water oxygen concentration and OPD are very likely to decline, suggesting that the rates of authigenic Mo and U uptake indirectly track redox-conditions at the seafloor. Despite this link between OM delivery and the depth of SMTZ, however, it is important to note that C_{org} may be decoupled from authigenic Mo and U in sediment compositional data (Fig. 6) since the solid-phase uptake of the two metals commences relatively deep within the sediment column.

To effectively assess the applicability of sedimentary Mo and U to

Table 3
Calculated diffusive fluxes (F) of Mo and U. Down arrows represent downward fluxes from the zone of OCR-Fe-Mn towards the SMTZ, where authigenic sequestration of Mo and U occurs. Plain numbers indicate diffusive fluxes between bottom waters and the SMTZ, while numbers in brackets represent diffusive fluxes at the upper boundary of the SMTZ caused by particulate shuttling. Up arrows denote deep-sourced upward fluxes. Estimates for average mass accumulation rates of authigenic (XS) Mo and U within the SMTZ are also shown. All values are given in μmol/m^2/yr.

Station	Mo_{xs} MAR	F_{Mo} ↓ 2016	F_{Mo} ↑ 2016	F_{Mo} ↓ 2017	U_{XS} MAR	F_U ↓ 2016	F_U ↑ 2016	F_U ↓ 2017
St 1	27.3	6.3 (28.5)	1.3	1.9 (21.4)	3.0	0.5	0.1	0.3
St 2	9.0	(11.7)		6.2	1.5	(1.4)		0.4
St 3	10.6	(9.2)			2.6	(0.6)	0.1	
St 4	18.8		3.1	(9.2)	4.5		0.5	0.3 (1.1)

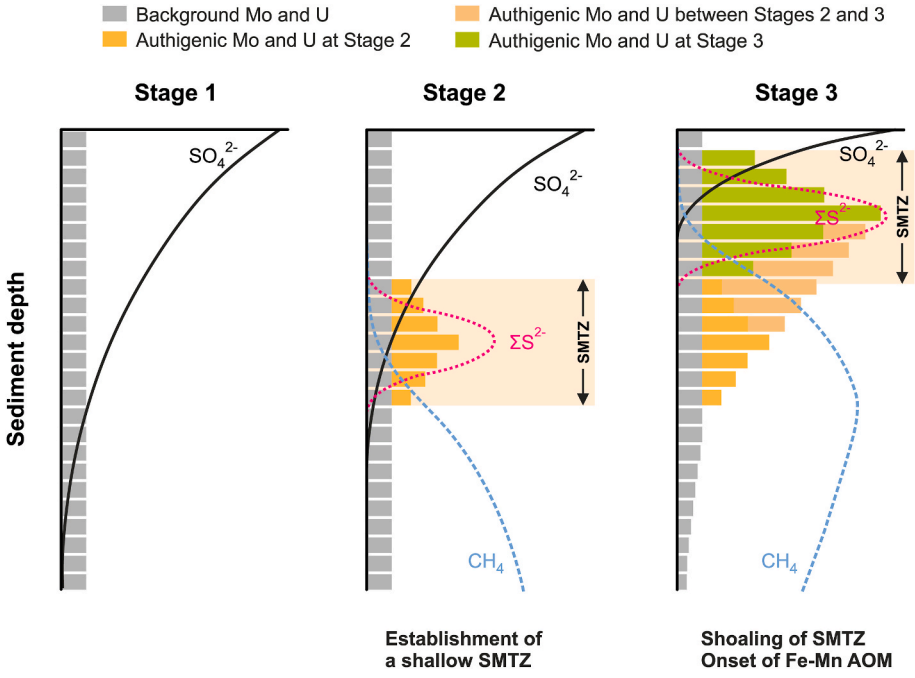

Fig. 7. Conceptual model for authigenic Mo and U sequestration over time in the study area. At Stage 1, the lack of a shallow SMTZ impedes authigenic Mo and U uptake. At Stage 2, a pronounced shallow SMTZ was established as a response to excess human-induced nutrient input in the first half of the 20th century, which initiated authigenic sequestration of Mo and U within the sulfidic front. At Stage 3, further aggravation of eutrophication and hypoxia driven by multiple feedback mechanisms and climatic warming stimulated shoaling and intensification of the SMTZs and initiation of Fe–Mn AOM since the 1950s, resulting in shallower and more efficient sequestration of Mo and U.

record past changes in bottom water oxygenation, it is necessary to outline the potential biases inherent in these records. For example, post-depositional remobilization, changes in the intensity of particulate shuttling, and variations in the lock-in-depth of the authigenic signal might compromise the viability of these redox records. Below we address the effects of these factors in detail.

4.5.2. Effects of particulate shuttling and deep-sourced supply of dissolved Mo and U

Particulate shuttling with Fe–Mn (oxyhydr)oxides might compromise the applicability of Mo and U as direct proxies for bottom water oxygenation in non-euxinic settings. Similarly to the seasonally anoxic Chesapeake Bay, we expect that the particulate shuttling-induced delivery of Mo associated with recycling of Fe–Mn (oxyhydr)oxides at our sites may become amplified with progressive deoxygenation (Eaton, 1979; Shaw et al., 1994; Adelson et al., 2001; Morford et al., 2007). This would lead to enhanced diffusive fluxes of Mo and U to the SMTZ with aggravation of hypoxia. The important implication of this is that particulate shuttling is likely to augment authigenic Mo and U sequestration upon declining oxygen levels in the bottom waters.

Similarly to particulate shuttling, the inferred upward diffusive fluxes of Mo and U to the SMTZ from a deep source could modulate the rate of authigenic Mo and U uptake irrespective of changes in bottom water oxygenation. However, temporal variations in the rate of Fe- (and likely also Mn) assisted AOM are primarily driven by vertical migrations in the diagenetic zonation, whereby shoaling of the SMTZ submerges reactive Fe oxides into the methanogenic zone and thus accelerates the process (Rooze et al., 2016). Analogously to the effects of particulate shuttling, this suggests that the deep-sourced flux of Mo and U is likely augmented with decreasing bottom water oxygen levels, thereby enhancing authigenic sequestration of Mo and U (Fig. 7).

4.5.3. Effects of lock-in-depth and post-depositional remobilization

Another important aspect that requires consideration when assessing the applicability of Mo and U as recorders of hypoxia is the lock-in-depth of the signal, i.e. the sediment depth where most of the authigenic sequestration commences. The observed decimeter-scale vertical offset between the SWI and the zone of authigenic Mo and U sequestration (corresponding to sedimentation over multiple decades) requires caution in the direct interpretation of high-resolution sediment profiles as records of bottom-water oxygenation at the time of accumulation of a given sediment horizon. In addition, upon vertical migrations of the SMTZ, the amount of authigenic Mo and U sequestration at any given depth likely integrates their uptake over multiple different stages (Fig. 7), which must be considered when assessing how changes in oxygenation have evolved. For seasonally hypoxic coastal areas, this implies that the annual variability of seafloor oxygenation is likely beyond the resolution of sedimentary Mo and U records.

Although post-depositional remobilization of authigenic Mo and U might theoretically bias their ability to track past changes in bottom water conditions, the positive mass balances (MARs of Mo_{XS} and U_{XS} > diffusive fluxes) for both metals suggest that their authigenic phases are effectively retained in the solid-phase. Based on the sequential extractions, a major proportion of the authigenic Mo is largely unreactive (F5)

and likely preserved in sedimentary records over geological time scales. Indeed, oxidative dissolution of authigenic Mo in F5 is highly unlikely due to the irreversibility of the key processes preceding Mo fixation, including the sulfidation of MoO_4^{2-} (Erickson and Helz, 2000), MoS_4^{2-} adsorption on pyrite surfaces (Bostick et al., 2003) and the precipitation of $FeMoS_4$ (Vorlicek et al., 2018). However, the proportion of Mo_{XS} that resides in F1 is extremely labile, and hence permanent burial of this Mo pool is predicated upon the potential conversion into more refractory phases in the course of diagenesis. Nonetheless, if indeed Mo in F1 is hosted by sulfidized OM, we expect that at least part of this Mo pool converts into more refractory forms in the course of diagenesis, as evidenced by the widespread preservation of such compounds in ancient marine sediments (Helz et al., 1996; Tribovillard et al., 2004).

Similarly to Mo, the authigenic U in F5 (uraninite and pyrite-hosted) likely remains stable during diagenesis, while that in F2 (monomeric U (IV)) is expected to be more prone to oxidative dissolution (Wan et al., 2005; Cerrato et al., 2013; Alessi et al., 2014; Newsome et al., 2015). Accordingly, seasonal downward migrations of the SMTZ might result in oxidative dissolution of the authigenic U phases (Shaw et al., 1994; Zheng et al., 2002a; Morford et al., 2009b). Nonetheless, the broadly stagnant vertical position of the zone of reductive Fe dissolution between different seasons (Fig. 3; Myllykangas et al., 2020a) suggests that such oxygenation events are of minor importance. We also note that localized oxidation caused by bioirrigation might mobilize U in F2 (Zheng et al., 2002a; Morford et al., 2009a), but this is unlikely at our study sites since the authigenic U uptake commences within the SMTZ, where burrowing by macrobenthic fauna is effectively prevented by the relatively high ΣS^{2-} levels (Fig. 5; Diaz and Rosenberg, 1995).

4.5.4. *A conceptual model for authigenic Mo and U sequestration in non-euxinic coastal settings with a shallow SMTZ*

In Fig. 7 we have compiled the evolution of authigenic Mo and U sequestration in a scenario relevant for the coastal Baltic Sea (cf. Jokinen et al., 2018). *Stage 1* in the scenario represents the period prior to eutrophication (before the 20th century), when authigenic uptake of Mo and U was negligible due to the absence of a shallow SMTZ. In the first half of the 20th century (*Stage 2*), excess anthropogenic nutrient loading from the catchment augmented the delivery of OM to the sediments, thereby causing establishment of a shallow SMTZ and onset of authigenic Mo and U uptake. Since the 1950s, intensification of agricultural practices and climatic warming have aggravated eutrophication and hypoxia (*Stage 3*), promoting substantial shoaling and amplification of the STMZ and onset of Fe–Mn-mediated AOM, hence further enhancing the authigenic sequestration of Mo and U. Despite the reductions in anthropogenic nutrient loading in the 21st century, feedback mechanisms associated with eutrophication and hypoxia (Vahtera et al., 2007; McCrackin et al., 2018) together with the large pool of reactive OM accumulated over the past decades are likely to sustain a shallow SMTZ and effective Mo and U sequestration for decades. The Mo and U enrichments that result from this sequence of events are strongly focused into a single large peak representing the mature position of the SMTZ (Fig. 7).

We postulate that this conceptual model for authigenic Mo and U sequestration in response to the shoaling of the SMTZ could be applicable not only in the coastal Baltic Sea but also in other low-salinity systems affected by anthropogenic eutrophication and associated bottom water deoxygenation. However, we caution that global-scale inter-site comparisons of bottom water oxygenation solely based on Mo_{XS} and U_{XS} will be complicated due to the number of site-specific factors that modulate the absolute rate of the authigenic sequestration (Algeo and Li, 2020; Algeo and Liu, 2020). For example, sedimentation rate modulates the amplitude of trace metal enrichments (e.g. Sageman et al., 2003; Lyons and Kashgarian, 2005; Liu and Algeo, 2020), underlining that the accuracy of inter-site comparisons can be significantly improved by assessing the MARs of Mo_{XS} and U_{XS}. Yet, our model implies that long term (multi-decadal or longer) fluctuations in Mo_{XS} and U_{XS} in any given coastal setting qualitatively track past fluctuations in the bottom water oxygenation through its influence on the depth of the SMTZ.

5. Conclusions

This study sheds light on the mechanisms of authigenic sequestration of Mo and U in a eutrophic, low-salinity coastal setting, where high rates of OM deposition have led to a shallow positioning of the SMTZ within the sediment column. Authigenic uptake of the two metals is triggered within the SMTZ, where dissolved sulfide accumulation increases the particle affinity of dissolved Mo and U species, hence reducing their solubility. Our results emphasize the key role of the depth and intensity of the SMTZ in dictating the rate of authigenic sequestration of both Mo and U, whereby shoaling of the diagenetic zonation catalyzes their uptake.

Based on our sequential extraction results, the majority of the authigenic Mo resides in pyrite and/or nanoscale $FeMoS_4$ precipitates in the residual fraction, evidencing that Mo uptake is dominated by the Fe sulfide pathway. However, part of the Mo pool is extremely labile, potentially recording an intermediate phase in the authigenic sequestration process. The host phases and the ultimate fate of this labile Mo pool remain elusive, but we infer that the occurrence of these Mo species might reflect formation of organic thiomolybdates upon thiolation of OM deep within the SMTZ, where dissolved Fe levels remain low. Similarly to Mo, the speciation of authigenic U is bimodal; part of this pool dissolved already in the second stage of our sequential extraction scheme, while the rest was substantially more refractory and resided in the residual fraction. We infer that the refractory phases record authigenic U uptake mainly in the form of crystalline uraninite, whereas the more labile phases are comprised of monomeric U(IV) principally associated with biomass. Based on the close coupling between U_{XS} and pore water ΣS^{2-}, sequestration of U into both of these authigenic pools is plausibly linked to accumulation of dissolved sulfide.

Our results strongly suggest that authigenic forms of Mo and U remain largely immobile in the sediment, signaling their potential to track past changes in bottom water oxygenation. In a broad context, our findings suggest an indirect link between deoxygenation and authigenic sequestration of Mo and U in eutrophic low-salinity coastal settings, since shoaling of the SMTZ is often accompanied by decreasing bottom water oxygen levels. However, while these proxies are potentially viable paleo-redox recorders within a given coastal area, the multitude of other site-specific forcing factors renders global-scale comparisons of bottom water oxygenation between different coastal settings merely based on authigenic Mo and U uptake unfeasible. In addition, the temporal resolution of Mo- and U-based redox reconstructions in these environments is compromised by their deep and potentially time-variant depth of sequestration, which should be considered when assessing past changes in the intensity of hypoxia.

Funding

This work was funded by the Academy of Finland [grant numbers 278827, 304006, 312495, 317684, 319956] and the Finnish Cultural Foundation [grant number 00190397].

Author contribution

Sami Jokinen: Writing – original draft, Formal analysis, Conceptualization, Investigation. Karoliina Koho: Writing – review and editing, Conceptualization, Supervision, Funding acquisition, Investigation. Joonas Virtasalo: Writing – review and editing, Supervision, Investigation. Tom Jilbert: Writing – review and editing, Conceptualization, Methodology, Supervision, Funding acquisition, Investigation.

Conflict of interest

The authors declare no conflict of interest.

Declaration of competing interest

The authors declare that they have no known competing financial interests or personal relationships that could have appeared to influence the work reported in this paper.

Acknowledgements

The authors would like to thank the Tvärminne Zoological Station in their valuable support during the field campaigns and subsequent nutrient and carbon analyses. Specifically we would like to acknowledge Göran Lundberg, Veijo Kinnunen, Tero Mustonen, Hanna Halonen, Jaana Koistinen, Antti Nevalainen, and Mervi Sjöblom. We also thank Iines Salonen, Myrsini Chronopoulou, and Pirita Anttila for their help during the sediment sampling and processing in the field. Rosa Tiihonen-Filppula is specifically thanked for conducting the sequential extraction work. Utrecht University GeoLab, especially Helen de Waard, is acknowledged for performing the ICP-MS analyses. This study has utilized research infrastructure facilities provided by FINMARI (Finnish Marine Research Infrastructure network).

Appendix A. Supplementary data

Supplementary data to this article can be found online at https://doi.org/10.1016/j.apgeochem.2020.104767.

References

Adelson, J.M., Helz, G.R., Miller, C.V., 2001. Reconstructing the rise of recent coastal anoxia; molybdenum in Chesapeake Bay sediments. Geochem. Cosmochim. Acta 65 (2), 237–252. https://doi.org/10.1016/S0016-7037(00)00539-1.

Alessi, D.S., Lezama-Pacheco, J.S., Janot, N., Suvorova, E.I., Cerrato, J.M., Giammar, D. E., Davis, J.A., Fox, P.M., Williams, K.H., Long, P.E., Handley, K.M., Bernier-Latmani, R., Bargar, J.R., 2014. Speciation and reactivity of uranium products formed during *in situ* bioremediation in a shallow alluvial aquifer. Environ. Sci. Technol. 48, 12842–12850. https://doi.org/10.1021/es502701u.

Alessi, D.S., Uster, B., Veeramani, H., Suvorova, E.I., Lezama-Pacheco, J.S., Stubbs, J.E., Bargar, J.R., Bernier-Latmani, R., 2012. Quantitative separation of monomeric U(IV) from UO_2 in products of U(VI) reduction. Environ. Sci. Technol. 46, 6150–6157. https://doi.org/10.1021/es204123z.

Algeo, T.J., Li, C., 2020. Redox classification and calibration of redox thresholds in sedimentary systems. Geochem. Cosmochim. Acta. https://doi.org/10.1016/j.gca.2020.01.055.

Algeo, T.J., Liu, J., 2020. A re-assessment of elemental proxies for paleoredox analysis. Chem. Geol. 540, 119549. https://doi.org/10.1016/j.chemgeo.2020.119549.

Algeo, T.J., Lyons, T.W., 2006. Mo–total organic carbon covariation in modern anoxic marine environments: implications for analysis of paleoredox and paleohydrographic conditions. Paleoceanography 21, PA1016. https://doi.org/10.1029/2004PA001112.

Algeo, T.J., Tribovillard, N., 2009. Environmental analysis of paleoceanographic systems based on molybdenum–uranium covariation. Chem. Geol. 268 (3–4), 211–225. https://doi.org/10.1016/j.chemgeo.2009.09.001.

Anderson, R.F., 1987. Redox behavior of uranium in an anoxic marine basin. Uranium 3, 145–164.

Arndt, S., Jørgensen, B.B., LaRowe, D.E., Middelburg, J.J., Pancost, R.D., Regnier, P, 2013. Quantifying the degradation of organic matter in marine sediments: A review and synthesis. Earth Sci. Rev. 123, 53–86. https://doi.org/10.1016/j.earscirev.2013.02.008.

Bargar, J.R., Williams, K.H., Campbell, K.M., Long, P.E., Stubbs, J.E., Suvorova, E.I., Lezama-Pacheco, J.S., Alessi, D.S., Stylo, M., Webb, S.M., Davis, J.A., Giammar, D.E., Blue, L.Y., Bernier-Latmani, R., 2013. Uranium redox transition pathways in acetate-amended sediments. Proc. Natl. Acad. Sci. U. S. A 110 (12), 4506–4511. https://doi.org/10.1073/pnas.1219198110.

Beal, E.J., House, C.H., Orphan, V.J., 2009. Manganese and iron dependent marine methane oxidation. Science 325, 184–187. https://doi.org/10.1126/science.1169984.

Bennett, W.W., Canfield, D.E., 2020. Redox-sensitive trace metals as paleoredox proxies: a review and analysis of data from modern sediments. Earth Sci. Rev. 204, 103175. https://doi.org/10.1016/j.earscirev.2020.103175.

Bernier-Latmani, R., Veeramani, H., Vecchia, E.D., Junier, P., Lezama-Pacheco, J.S., Suvorova, E.I., Sharp, J.O., Wigginton, N.S., Bargar, J.R., 2010. Non-uraninite products of microbial U(VI) reduction. Environ. Sci. Technol. 44, 945–9462. https://doi.org/10.1021/es101675a.

Bhattacharyya, A., Campbell, K.M., Kelly, S.D., Roebbert, Y., Weyer, S., Bernier-Latmani, R., Borch, T., 2017. Biogenic non-crystalline U(IV) revealed as major component in uranium ore deposits. Nat. Commun. 8, 15538. https://doi.org/10.1038/ncomms15538.

Boetius, A., Ravenschlag, K., Schubert, C.J., Rickert, D., Widdel, A., Amann, R., Jørgensen, B.B., Witte, U., Pfannkuche, O., 2000. A marine microbial consortium apparently mediating anaerobic oxidation of methane. Nature 407, 623–626. https://doi.org/10.1038/35036572.

Bonaglia, S., Bartoli, M., Gunnarsson, J.S., Rahm, L., Raymond, C., Svensson, O., Yekta, S., Brüchert, V., 2013. Effect of reoxygenation and Marenzelleria spp. bioturbation on Balti Sea sediment metabolism. Mar. Ecol. Prog. Ser. 482, 43–55. https://doi.org/10.3354/meps10232.

Bone, S.E., Dynes, J.J., Cliff, J., Bargar, J.R., 2017. Uranium(IV) adsorption by natural organic matter in anoxic sediments. Proc. Natl. Acad. Sci. U. S. A 114 (4), 711–716. https://doi.org/10.1073/pnas.1611918114.

Bordas, F., Bourg, A.C.M., 1998. A critical evaluation of sample pretreatment for storage of contaminated sediments to be investigated for the potential mobility of their heavy metal load. Water Air Soil Pollut. 103, 137–149. https://doi.org/10.1023/A:1004952608950.

Bostick, B.C., Fendorf, S., Helz, G.R., 2003. Differential adsorption of molybdate and tetrathiomolybdate on pyrite (FeS_2). Environ. Sci. Technol. 37, 285–291. https://doi.org/10.1021/es303138d.

Boudreau, B.P., 1996. The diffusive tortuosity of fine-grained unlithified sediments. Geochem. Cosmochim. Acta 60 (16), 3139–3142. https://doi.org/10.1016/0016-7037(96)00158-5.

Boudreau, B.P., 1997. Diagenetic Models and Their Implementation. Springer, p. 414p. https://doi.org/10.1007/978-3-642-60421-8 pp.

Boyanov, M.I., Fletcher, K.E., Kwon, M.J., Rui, X., O'Loughlin, E.J., Löffler, F.E., Kemner, K.M., 2011. Solution and microbial controls on the formation of reduced U (IV) species. Environ. Sci. Technol. 45, 8336–8344. https://doi.org/10.1021/es2014049.

Breitburg, D., Levin, L.A., Oschlies, A., Grégoire, M., Chavez, F.P., Conley, D.J., Garçon, V., Gilbert, D., Gutiérrez, D., Isensee, K., Jacinto, G.S., Limburg, K.E., Montes, I., Naqvi, S.W.A., Pitcher, G.C., Rabalais, N.N., Roman, M.R., Rose, K.A., Seibel, B.A., Telszewski, M., Yasuhara, M., Zhang, J., 2018. Declining oxygen in the global ocean and coastal waters. Science 359. https://doi.org/10.1126/science.aam7240 eaam7240.

Brennecka, G.A., Wasylenski, L.E., Bargar, J.R., Weyer, S., Anbar, A.D., 2011. Uranium isotope fractionation during adsorption to Mn-oxyhydroxides. Environ. Sci. Technol. 45, 1370–1375. https://doi.org/10.1021/es103061v.

Bura-Nakić, E., Andersen, M.B., Archer, C., de Souza, G.F., Margus, M., Vance, D., 2018. Coupled Mo-U abundances and isotopes in a small marine euxinic basin: constraints on processes in euxinic basins. Geochem. Cosmochim. Acta 222, 212–229. https://doi.org/10.1016/j.gca.2017.10.023.

Burton, E.D., Sullivan, L.A., Bush, R.T., Johnston, S.G., Keene, A.F., 2008. A simple and inexpensive chromium-reducible sulfur method for acid-sulfate soils. Appl. Geochem. 23 (9), 2759–2766. https://doi.org/10.1016/j.apgeochem.2008.07.007.

Cerrato, J.M., Ashner, M.N., Alessi, D.S., Leza-Pacheco, J.S., Bernier-Latmani, R., Bargar, J.R., Giammar, D.E., 2013. Relative reactivity of biogenic and chemogenic uraninite and biogenic noncrystalline U(IV). Environ. Sci. Technol. 47, 9756–9763. https://doi.org/10.1021/es401663t.

Chaillou, G., Anschutz, P., Lavaux, G., Schäfer, J., Blanc, G., 2002. The distribution of Mo, U, and Cd in relation to major redox species in muddy sediments of the Bay of Biscay. Mar. Chem. 80 (1), 41–59. https://doi.org/10.1016/S0304-4203(02)00097-X.

Cline, J., 1969. Spectrophotometric determination of hydrogen sulfide in natural waters. Limnol. Oceanogr. 14 (3), 454–458. https://doi.org/10.4319/lo.1969.14.3.0454.

Cooper, S.R., Brush, G.S., 1991. Long-term history of Chesapeake bay anoxia. Science 254, 991–996. https://doi.org/10.1126/science.254.5034.992.

Cornwell, J.C., Morse, J.W., 1987. The characterization of iron sulfide minerals in anoxic marine sediments. Mar. Chem. 22 (2–4), 193–206. https://doi.org/10.1016/0304-4203(87)90008-9.

Dahl, T.W., Anbar, A.D., Gordon, G.W., Rosing, M.T., Frei, R., Canfield, D.E., 2010. The behavior of molybdenum and its isotopes across the chemocline and in the sediments of sulfidic Lake Cadagno, Switzerland. Geochem. Cosmochim. Acta 74 (1), 144–163. https://doi.org/10.1016/j.gca.2009.09.018.

Dahl, T.W., Chappaz, A., Fitts, J.P., Lyons, T.W., 2013. Molybdenum reduction in a sulfidic lake: evidence from X-ray absorption fine-structure spectroscopy and implications for the Mo paleoproxy. Geochem. Cosmochim. Acta 103, 213–231. https://doi.org/10.1016/j.gca.2012.10.058.

Dahl, T.W., Chappaz, A., Hoek, J., McKenzie, C.J., Svane, S., Canfield, D.E., 2017. Evidence of molybdenum association with particulate organic matter under sulfidic conditions. Geobiology 15 (2), 311–323. https://doi.org/10.1111/gbi.12220.

Dang, D.H., Novotnik, B., Wang, W., Georg, R.B., Evans, R.D., 2016. Uranium isotope fractionation during adsorption (co)precipitation, and biotic reduction. Environ. Sci. Technol. 50, 12695–12704. https://doi.org/10.1021/acs.est.6b01459.

Descostes, M., Schlegel, M.L., Eglizaud, N., Descamps, F., Miserque, F., Simoni, E., 2010. Uptake of uranium and trace elements in pyrite (FeS_2) suspensions. Geochem. Cosmochim. Acta 74 (5), 1551–1562. https://doi.org/10.1016/j.gca.2009.12.004.

Diaz, R.J., Rosenberg, R., 1995. Marine benthic hypoxia: a review of its ecological effects and the behavioural responses of benthic macrofauna. Oceanogr. Mar. Biol. Annu. Rev. 33, 245–303.

Diaz, R.J., Rosenberg, R., 2008. Spreading of dead zones and consequences for marine ecosystems. Science 321, 926–929. https://doi.org/10.1126/science.1156401.

Eaton, A., 1979. The impact of anoxia on Mn fluxes in the Chesapeake Bay. Geochem. Cosmochim. Acta 43 (3), 429–432. https://doi.org/10.1016/0016-7037(79)90208-4.

Edelman, N., 1949. Structural history of the eastern part of the Gullkrona Basin, SW-Finland. Bull. Comm. Geol. Finl. 148, 1–48.

Egger, M., Rasigraf, O., Sapart, C.J., Jilbert, T., Jetten, M.S.M., Rockmann, T., van der Veen, C., Banda, N., Kartal, B., Ettwig, K.F., Slomp, C.P., 2015. Iron-mediated anaerobic oxidation of methane in brackish coastal sediments. Environ. Sci. Technol. 49, 277–283. https://doi.org/10.1021/es503663z.

Emerson, S.R., Huested, S.S., 1991. Ocean anoxia and the concentrations of molybdenum and vanadium in seawater. Mar. Chem. 34 (3–4), 177–196. https://doi.org/10.1016/0304-4203(91)90002-E.

Erhardt, A.M., Reimers, C.E., Kadko, D., Paytan, A., 2014. Records of trace metals in sediments from the Oregon shelf and slope: investigating the occurrence of hypoxia over the past several thousand years. Chem. Geol. 382, 32–43. https://doi.org/10.1016/j.chemgeo.2014.05.029.

Erickson, B.E., Helz, G.R., 2000. Molybdenum(VI) speciation in sulfidic waters: stability and lability of thiomolybdates. Geochem. Cosmochim. Acta 64 (7), 1149–1158. https://doi.org/10.1016/S0016-7037(99)00423-8.

Fennel, K., Testa, J.M., 2018. Biogeochemical controls on coastal hypoxia. Annual Review of Marine Science 11, 105–130. https://doi.org/10.1146/annurev-marine-010318-095138.

Fleming-Lehtinen, V., Räike, A., Kortelainen, P., Kauppila, P., Thomas, D.N., 2015. Organic carbon concentration in the northern coastal Baltic Sea between 1975 and 2011. Estuar. Coast 38, 466–481. https://doi.org/10.1007/s12237-014-9829-y.

Freund, C., Wishard, A., Brenner, R., Sobel, M., Mizelle, J., Kim, A., Meyer, D.A., Morford, J.L., 2016. The effect of a thiol-containing organic molecule on molybdenum adsorption onto pyrite. Geochem. Cosmochim. Acta 174, 222–235. https://doi.org/10.1016/j.gca.2015.11.015.

Froelich, P.N., Klinkhammer, G.P., Bender, M.L., Luedtke, N.A., Heath, G.R., Cullen, D., Dauphin, P., 1979. Early oxidation of organic matter in pelagic organic sediments of the eastern equatorial Atlantic: suboxic diagenesis. Geochem. Cosmochim. Acta 43 (7), 1075–1090. https://doi.org/10.1016/0016-7037(79)90095-4.

Fu, H., Zhang, H., Sui, Y., Hu, N., Ding, D., Ye, Y., Li, G., Wang, Y., Dai, Z., 2018. Transformation of uranium species in soil during redox oscillations. Chemosphere 208, 846–853. https://doi.org/10.1016/j.chemosphere.2018.06.059.

Gallegos, T.J., Fuller, C.C., Webb, S.M., Betterton, W., 2013. Uranium(VI) interactions with mackinawite in the presence and absence of bicarbonate and oxygen. Environ. Sci. Technol. 47, 7357–7364. https://doi.org/10.1021/es400450z.

Goñi, M., Teixeira, M., Perkey, D., 2003. Sources and distribution of organic matter in a river dominated estuary (Winyah Bay, SC, USA). Estuar. Coast Shelf Sci. 57 (5–6), 1023–1048. https://doi.org/10.1016/S0272-7714(03)00008-8.

Gooday, A.J., Jorissen, F., Levin, L.A., Middelburg, J.J., Naqvi, S.W.A., Rabalais, N.N., Scranton, M., Zhang, J., 2009. Historical records of coastal eutrophication-induced hypoxia. Biogeosciences 6, 1707–1745. https://doi.org/10.5194/bg-6-1707-2009.

Helz, G.R., Adelson, J.M., 2013. Trace element profiles in sediments as redox proxies of dead zone history; rhenium compared to molybdenum. Environ. Sci. Technol. 47, 1257–1264. https://doi.org/10.1021/es303138d.

Helz, G.R., Bura-Nakić, E., Mikac, N., Ciglenečki, I., 2011. New model for molybdenum behavior in euxinic waters. Chem. Geol. 284 (3–4), 323–332. https://doi.org/10.1016/j.chemgeo.2011.03.012.

Helz, G.R., Miller, C.V., Charnock, J.M., Mosselmans, J.F.W., Pattrick, R.A.D., Garner, C. D., Vaughan, D.J., 1996. Mechanism of molybdenum removal from the sea and its concentration in black shales: EXAFS evidence. Geochem. Cosmochim. Acta 60 (19), 3631–3642. https://doi.org/10.1016/0016-7037(96)00195-0.

Helz, G.R., Vorlicek, T.P., 2019. Precipitation of molybdenum from euxinic waters and the role of organic matter. Chem. Geol. 509, 178–193. https://doi.org/10.1016/j.chemgeo.2019.02.001.

Helz, G.R., Vorlicek, T.P., Kahn, M.D., 2004. Molybdenum scavenging by iron monosulfide. Environ. Sci. Technol. 4263–4268. https://doi.org/10.1021/es034969+, 2004.

Hietanen, S., Kuparinen, J., 2008. Seasonal and short-term variation in denitrification and anammox at a coastal station on the Gulf of Finland, Baltic Sea. Hydrobiologia 596 (1), 67–77. https://doi.org/10.1007/s10750-007-9058-5.

Hjorth, T., 2004. Effects of freeze-drying on partitioning patterns of major elements and trace metals in lake sediments. Anal. Chim. Acta 526, 95–102. https://doi.org/10.1016/j.aca.2004.08.007.

Hoffmann, A.F., Soetaert, K., Middelburg, J.J., Meysman, F.J.R., 2010. AquaEnv: an aquatic acid–base modelling environment in R. Aquat. Geochem. 16 (4), 507–546. https://doi.org/10.1007/s10498-009-9084-1.

Holby, O, Evans, S, 1996. The vertical distribution of Chernobyl-derived radionuclides in a Baltic Sea sediment. J. Environ. Radioact. 33 (2), 129–145. https://doi.org/10.1016/0265-931X(95)00089-S.

Holmden, C., Amini, M., Francois, R., 2015. Uranium isotope fractionation in Saanich Inlet: a modern analog study of a paleoredox tracer. Geochem. Cosmochim. Acta 153, 202–215. https://doi.org/10.1016/j.gca.2014.11.012.

Hua, B., Xu, H., Terry, J., Deng, B., 2006. Kinetics of uranium(VI) reduction by hydrogen sulfide in anoxic aqueous systems. Environ. Sci. Technol. 40, 4666–4671. https://doi.org/10.1021/es051804n.

Huang, G., Chen, Z., Sun, J., Liu, F., Wang, J., Zhang, Y., 2015. Effect of sample pretreatment on the fractionation of arsenic in anoxic soils. Environ. Sci. Pollut. Control Ser. 22, 8367–8374. https://doi.org/10.1007/s11356-014-3958-5.

Huerta-Diaz, M.A., Morse, J.W., 1992. Pyritization of trace metals in anoxic marine sediments. Geochem. Cosmochim. Acta 56 (7), 2681–2702. https://doi.org/10.1016/0016-7037(92)90353-K.

Hyun, S.P., Davis, J.A., Sun, K., Hayes, K.F., 2012. Uranium(VI) reduction by iron(II) monosulfide mackinawite. Environ. Sci. Technol. 46, 3369–3376. https://doi.org/10.1021/es203786p.

Jilbert, T., Slomp, C.P., 2013a. Rapid high-amplitude variability in Baltic Sea hypoxia during the holocene. Geology 41 (11), 1183–1186. https://doi.org/10.1130/G34804.1.

Jilbert, T., Slomp, C.P., 2013b. Iron and manganese shuttles control the formation of authigenic phosphorus minerals in the euxinic basins of the Baltic Sea. Geochem. Cosmochim. Acta 107, 155–169. https://doi.org/10.1016/j.gca.2013.01.005.

Jilbert, T., Asmala, E., Schröder, C., Tiihonen, R., Myllykangas, J.-P., Virtasalo, J.J., Kotilainen, A., Peltola, P., Ekholm, P., Hietanen, S., 2018. Impacts of flocculation on the distribution and diagenesis of iron in boreal estuarine sediments. Biogeosciences 15, 1243–1271. https://doi.org/10.5194/bg-15-1243-2018.

Jokinen, S.A., Jilbert, T., Tiihonen-Filppula, R., Koho, K., 2020. Terrestrial organic matter input drives sedimentary trace metal sequestration in a human-impacted boreal estuary. Sci. Total Environ. 717, 137047. https://doi.org/10.1016/j.scitotenv.2020.137047.

Jokinen, S.A., Virtasalo, J.J., Jilbert, T., Kaiser, J., Dellwig, O., Arz, H.W., Hänninen, J., Arppe, L., Collander, M., Saarinen, T., 2018. A 1500-year multiproxy record of coastal hypoxia from the northern Baltic Sea indicates unprecedented deoxygenation over the 20th century. Biogeosciences 15, 3975–4001. https://doi.org/10.5194/bg-15-3975-2018.

Jokinen, S.A., Virtasalo, J.J., Kotilainen, A.T., Saarinen, T., 2015. Varve microfabric record of seasonal sedimentation and bottom flow-modulated mud deposition in the coastal northern Baltic Sea. Mar. Geol. 366, 79–96. https://doi.org/10.1016/j.margeo.2015.05.003.

Jørgensen, B.B., Beulig, F., Egger, M., Petro, C., Scholze, C., Røy, H., 2019. Organoclastic sulfate reduction in the sulfate-methane transition of marine sediments. Geochem. Cosmochim. Acta 254, 231–245. https://doi.org/10.1016/j.gca.2019.03.016.

Kauppi, L., Norkko, A., Norkko, J., 2018. Seasonal population dynamics of the invasive polychaete genus Marenzelleria spp. in contrasting soft-sediment habitats. J. Sea Res. 131, 46–60. https://doi.org/10.1016/j.seares.2017.10.005.

Kersten, M., Förstner, U., 1986. Chemical fractionation of heavy metals in anoxic estuarine and coastal sediments. Water Sci. Technol. 18 (4–5), 121–130. https://doi.org/10.2166/wst.1986.0187.

Klaminder, J, Appleby, P, Crook, P, Renberg, I, 2012. Post-deposition diffusion of ^{137}Cs in lake sediment: Implications for radiocaesium dating. Sedimentology 59 (7), 2259–2267. https://doi.org/10.1111/j.1365-3091.2012.01343.x.

Klinkhammer, G.P., Palmer, M.R., 1991. Uranium in the oceans: where it goes and why. Geochem. Cosmochim. Acta 55 (7), 1799–1806. https://doi.org/10.1016/0016-7037(91)90024-Y.

Koistinen, J., Sjöblom, M., Spilling, K., 2018. Determining inorganic and organic nitrogen. In: Methods in Molecular Biology. Humana Press, New York, USA, pp. 1–10. https://doi.org/10.1007/7651_2018_128.

Lalonde, K., Mucci, A., Ouellet, A., Gélinas, Y., 2012. Preservation of organic matter in sediments promoted by iron. Nature 483, 198–200. https://doi.org/10.1038/nature10855.

Langmuir, D., 1978. Uranium solution-mineral equilibria at low temperatures with applications to sedimentary ore deposits. Geochem. Cosmochim. Acta 42 (6), 547–569. https://doi.org/10.1016/0016-7037(78)90001-7.

Lee, S.Y., Baik, M.H., Cho, H.-R., Jung, E.C., Jeong, J.T., Choi, J.W., Lee, Y.B., Lee, Y.J., 2013. Abiotic reduction of uranium by mackinawite (FeS) biogenerated under sulfate-reducing condition. J. Radioanal. Nucl. Chem. 296, 1311–1319. https://doi.org/10.1007/s10967-013-2438-6.

Levin, L.A., Ekau, W., Gooday, A.J., Jorissen, F., Middelburg, J.J., Naqvi, S.W.A., Neira, C., Rabalais, N.N., Zhang, J., 2009. Effects of natural and human-induced hypoxia on coastal benthos. Biogeosciences 6, 2063–2098. https://doi.org/10.5194/bg-6-2063-2009.

Li, Y.-H., Gregory, S., 1974. Diffusion of ions in sea water and in deep-sea sediments. Geochem. Cosmochim. Acta 38 (5), 703–714. https://doi.org/10.1016/0016-7037(74)90145-8.

Liu, J., Algeo, T.J., 2020. Beyond redox: control of trace-metal enrichment in anoxic marine facies by watermass chemistry and sedimentation rate. Geochem. Cosmochim. Acta. https://doi.org/10.1016/j.gca.2020.02.037.

Löfvendahl, R., 1987. Dissolved uranium in the Baltic Sea. Mar. Chem. 21, 213–227. https://doi.org/10.1016/0304-4203(87)90060-0.

Lovley, D.R., Phillips, E.J.P., 1992. Reduction of uranium by *Desulfovibrio desulfuricans*. Appl. Environ. Microbiol. 58 (3), 850–856.

Lovley, D.R., Phillips, E.J.P., Gorby, Y.A., Landa, E.R., 1991. Microbial reduction of uranium. Nature 350, 413–416. https://doi.org/10.1038/350413a0.

Lyons, T.W., Anbar, A.D., Severmann, S., Scott, C., Gill, B.C., 2009. Tracking euxinia in the ancient ocean: a multiproxy perspective and Proterozoic case study. Annu. Rev. Earth Planet Sci. 37, 507–534. https://doi.org/10.1146/annurev.earth.36.031207.124233.

Lyons, T.W., Kashgarian, M., 2005. Paradigm lost, paradigm found: the Black Sea–black shale connection as viewed from the anoxic basin margin. Oceanography 18 (2), 86–99. https://doi.org/10.5670/oceanog.2005.44.

McCrackin, M.L., Muller-Karulis, B., Gustafsson, B.G., Howarth, R.W., Humborg, C., Svanbäck, A., Swaney, D.P., 2018. A century of legacy phosphorus dynamics in a large drainage basin. Global Biogeochem. Cycles 32 (7), 1107–1122. https://doi.org/10.1029/2018GB005914.

McLennan, S.M., 2001. Relationships between the trace element composition of sedimentary rocks and upper continental crust. G-cubed 2. https://doi.org/10.1029/2000GC000109, 2000GC000109.

McManus, J., Berelson, W.M., Severmann, S., Poulson, R.L., Hammond, D.E., Klinkhammer, G.P., Holm, C., 2006. Molybdenum and uranium geochemistry in

continental margin sediments: paleoproxy potential. Geochem. Cosmochim. Acta 70 (18), 4643–4662. https://doi.org/10.1016/j.gca.2006.06.1564.
McManus, J., Berelson, W.M., Klinkhammer, G.P., Hammond, D.E., Holm, C., 2005. Authigenic uranium: relationship to oxygen penetration depth and organic carbon rain. Geochem. Cosmochim. Acta 69 (1), 95–108. https://doi.org/10.1016/j.gca.2004.06.023.
Middelburg, J.J., Levin, L.A., 2009. Coastal hypoxia and sediment biogeochemistry. Biogeosciences 6, 1273–1293. https://doi.org/10.5194/bg-6-1273-2009.
Moffitt, S.E., Moffitt, R.A., Sauthoff, W., Davis, C.V., Hewett, K., Hill, T.M., 2015. Paleoceanographic insights on recent oxygen minimum zone expansion: lessons for modern oceanography. PloS One 10 (1), e0115246. https://doi.org/10.1371/journal.pone.0115246.
Morford, J.L., Emerson, S.R., Breckel, E.J., Kim, S.H., 2005. Diagenesis of oxyanions (V, U, Re, and Mo) in pore waters and sediments from a continental margin. Geochem. Cosmochim. Acta 69 (21), 5021–5032. https://doi.org/10.1016/j.gca.2005.05.015.
Morford, J.L., Martin, W.R., François, R., Carney, C.M., 2009a. A model for uranium, rhenium, and molybdenum diagenesis in marine sediments based on results from coastal locations. Geochem. Cosmochim. Acta 73 (10), 2938–2960. https://doi.org/10.1016/j.gca.2009.02.029.
Morford, J.L., Martin, W.R., François, R., Carney, C.M., 2009b. Uranium diagenesis in sediments underlying bottom waters with high oxygen content. Geochem. Cosmochim. Acta 73 (10), 2920–2937. https://doi.org/10.1016/j.gca.2009.02.014.
Morford, J.L., Martin, W.R., Kalnejais, L.H., François, R., Bothner, M., Karle, I.-M., 2007. Insights on geochemical cycling of U, Re and Mo from seasonal sampling in Boston Harbor, Massachusetts, USA. Geochem. Cosmochim. Acta 71 (4), 895–917. https://doi.org/10.1016/j.gca.2006.10.016.
Morgan, B., Rate, A.W., Burton, E.D., 2012. Trace element reactivity in FeS-rich estuarine sediments: influence of formation environment and acid sulfate soil drainage. Sci. Total Environ. 438, 463–476. https://doi.org/10.1016/j.scitotenv.2012.08.088.
Myllykangas, J.P., Hietanen, S., Jilbert, T., 2020a. Legacy effects of eutrophication on modern methane dynamics in a boreal estuary. Estuar. Coast 43, 189–206. https://doi.org/10.1007/s12237-019-00677-0.
Myllykangas, J.-P., Rissanen, A.J., Hietanen, S., Jilbert, T., 2020b. Influence of electron acceptor availability and microbial community structure on sedimentary methane oxidation in a boreal estuary. Biogeochemistry 148, 291–309. https://doi.org/10.1007/s10533-020-00660-z.
Nägler, T.F., Neubert, N., Böttcher, M.E., Dellwig, O., Schnetzer, B., 2011. Molybdenum isotope fractionation in pelagic euxinia: evidence from the modern Black and Baltic Seas. Chem. Geol. 289, 1–11. https://doi.org/10.1016/j.chemgeo.2011.07.001.
Newsome, L., Morris, K., Shaw, S., Trivedi, D., Lloyd, J.R., 2015. The stability of microbially reduced U(IV); impact of residual electron donor and sediment ageing. Chem. Geol. 409, 125–135. https://doi.org/10.1016/j.chemgeo.2015.05.016.
Noordmann, J., Weyer, S., Montoya-Pino, C., Dellwig, O., Neubert, N., Eckert, S., Paetzel, M., Böttcher, M.E., 2015. Uranium and molybdenum isotope systematics in modern euxinic basins: case studies from the central Baltic Sea and the Kyllaren fjord (Norway). Chem. Geol. 396, 182–195. https://doi.org/10.1016/j.chemgeo.2014.12.012.
Ojala, A.E.K., Luoto, T.P., Virtasalo, J.J., 2017. Establishing a high-resolution surface sediment chronology with multiple dating methods – testing 137Cs determination with Nurmijärvi clastic-biogenic varves. Quat. Geochronol. 37, 32–41. https://doi.org/10.1016/j.quageo.2016.10.005.
Poulton, S.W., Canfield, D.E., 2005. Development of a sequential extraction procedure for iron: implications for iron partitioning in continentally derived particulates. Chem. Geol. 214 (3–4), 209–221. https://doi.org/10.1016/j.chemgeo.2004.09.003.
Reese, B.K., Finneran, D.W., Mills, H.J., Zhu, M., Morse, J.W., 2011. Examination and refinement of the determination of aqueous hydrogen sulfide by the methylene blue method. Aquat. Geochem. 17, 567–582. https://doi.org/10.1007/s10498-011-9128-1.
Rickard, D., Luther III, G.W., 2007. Chemistry of iron sulfides. Chem. Rev. 107, 514–562. https://doi.org/10.1021/cr0503658.
Rickard, D., Morse, J.W., 2005. Acid volatile sulfide (AVS). Mar. Chem. 97 (3–4), 141–197. https://doi.org/10.1016/j.marchem.2005.08.004.
Rooze, J., Egger, M., Tsandev, I., Slomp, C.P., 2016. Iron-dependent anaerobic oxidation of methane in coastal surface sediments: potential controls and impact. Limnol. Oceanogr. 61, S267–S282. https://doi.org/10.1002/lno.10275.
Rozan, T.F., Theberge, S.M., Luther III, G., 2000. Quantifying elemental sulfur (S^0), bisulfide (HS^-) and polysulfides (S_x^{2-}) using a voltammetric method. Anal. Chim. Acta 415 (1–2), 175–184. https://doi.org/10.1016/S0003-2670(00)00844-8.
Ruttenberg, K.C., 1992. Development of a sequential extraction method for different forms of phosphorus in marine sediments. Limnol. Oceanogr. 37 (7), 1460–1482. https://doi.org/10.4319/lo.1992.37.7.1460.
Sageman, B.B., Murphy, A.E., Werne, J.P., Ver Straeten, C.A., Hollander, D.J., Lyons, T. W., 2003. A tale of shales: the relative roles of production, decomposition, and dilution in the accumulation of organic-rich strata, Middle-Upper Devonian, Appalachian basin. Chem. Geol. 195, 229–273. https://doi.org/10.1016/S0009-2541(02)00397-2.
Scheiderich, K., Helz, G.R., Walker, R.J., 2010. Century-long record of Mo isotopic composition in sediments of a seasonally anoxic estuary (Chesapeake Bay). Earth Planet Sci. Lett. 289 (1–2), 189–197. https://doi.org/10.1016/j.epsl.2009.11.008.
Scholz, F., Baum, M., Siebert, C., Eroglu, S., Dale, A.W., Naumann, M., Sommer, S., 2018. Sedimentary molybdenum cycling in the aftermath of seawater inflow to the intermittently euxinic Gotland Deep, Central Baltic Sea. Chem. Geol. 491, 27–38. https://doi.org/10.1016/j.chemgeo.2018.04.031.
Scholz, F., McManus, J., Sommer, S., 2013. The manganese and iron shuttle in a modern euxinic basin and implications for molybdenum cycling at euxinic ocean margins. Chem. Geol. 355, 56–68. https://doi.org/10.1016/j.chemgeo.2013.07.006.
Scholz, F., Neumann, T., 2007. Trace element diagenesis in pyrite-rich sediments of the Achterwasser lagoon, SW Baltic Sea. Mar. Chem. 107 (4), 516–532. https://doi.org/10.1016/j.marchem.2007.08.005.
Scholz, F., Siebert, C., Dale, A.W., Frank, M., 2017. Intense molybdenum accumulation in sediments underneath a nitrogenous water column and implications for the reconstruction of paleo-redox conditions based on molybdenum isotopes. Geochem. Cosmochim. Acta 213, 400–417. https://doi.org/10.1016/j.gca.2017.06.048.
Scott, C., Lyons, T.W., 2012. Contrasting molybdenum cycling and isotopic properties in euxinic versus non-euxinic sediments and sedimentary rocks: refining the paleoproxies. Chem. Geol. 324 (325), 19–27. https://doi.org/10.1016/j.chemgeo.2012.05.012.
Scott, T.B., Tort, O.R., Allen, G.C., 2007. Aqueous uptake of uranium onto pyrite surfaces; reactivity of fresh versus weathered material. Geochem. Cosmochim. Acta 71 (21), 5044–5053. https://doi.org/10.1016/j.gca.2007.08.017.
Senko, J.M., Kelly, S.D., Dohnalkova, A.C., McDonough, J.T., Kemner, K.M., Burgos, W. D., 2007. The effect of U(VI) bioreduction kinetics on subsequent reoxidation of biogenic U(IV). Geochem. Cosmochim. Acta 71 (19), 4644–4654. https://doi.org/10.1016/j.gca.2007.07.021.
Sharp, J.O., Lezama-Pacheco, J.S., Schofield, E.J., Junier, P., Ulrich, K.-U., Chinni, S., Veeramani, H., Margot-Roquier, C., Webb, S.M., Tebo, B.M., Giammar, D.E., Bargar, J.R., Bernier-Latmani, R., 2011. Uranium speciation and stability after reductive immobilization in aquifer sediments. Geochem. Cosmochim. Acta 75 (21), 6497–6510. https://doi.org/10.1016/j.gca.2011.08.022.
Sharp, J.O., Schofield, E.J., Veeramani, H., Suvorova, E.I., Kennedy, D.W., Marshall, M. J., Mehta, A., Bargar, J.R., Bernier-Latmani, R., 2009. Structural similarities between biogenic uraninites produced by phylogenetically and metabolically diverse bacteria. Environ. Sci. Technol. 43, 8295–8301. https://doi.org/10.1021/es901281e.
Shaw, T.J., Sholkovitz, E.R., Klinkhammer, G., 1994. Redox dynamics in the Chesapeake Bay: the effect of sediment-water uranium exchange. Geochem. Cosmochim. Acta 58 (14), 2985–2995. https://doi.org/10.1016/0016-7037(94)90173-2.
Slomp, C.P., Mort, H.P., Jilbert, T., Reed, D.C., Gustafsson, B.G., Wolthers, M., 2013. Coupled dynamics of iron and phosphorus in sediments of an oligotrophic coastal basin and the impact of anaerobic oxidation of methane. PloS One 8 (4), e62386. https://doi.org/10.1371/journal.pone.0062386.
Soetaert, K., Petzoldt, T., Meysman, F., 2010. Marelac: tools for aquatic sciences. R Package Version 2.1. https://CRAN.R-project.org/package=marelac.
Stylo, M., Neubert, N., Roebbert, Y., Weyer, S., Bernier-Latmani, R., 2015. Mechanism of uranium reduction and immobilization in desulfovibrio vulgaris biofilms. Environ. Sci. Technol. 49, 10553–10561. https://doi.org/10.1021/acs.est.5b01769.
Sulu-Gambari, F., Roepert, A., Jilbert, T., Hagens, M., Meysman, F.J.R., Slomp, C.P., 2017. Molybdenum dynamics in sediments of a seasonally-hypoxic coastal marine basin. Chem. Geol. 466, 627–640. https://doi.org/10.1016/j.chemgeo.2017.07.015.
Sundby, B., Martinez, P., Gobeil, C., 2004. Comparative geochemistry of cadmium, rhenium, uranium, and molybdenum in continental margin sediments. Geochem. Cosmochim. Acta 68 (11), 2485–2493. https://doi.org/10.1016/j.gca.2003.08.011.
Tessier, A., Campbell, P.G.C., Bisson, M., 1979. Sequential extraction procedure for the speciation of particulate trace metals. Anal. Chem. 51 (7), 844–851. https://doi.org/10.1021/ac50043a017.
Tribovillard, N., Algeo, T.J., Lyons, T., Riboulleau, A., 2006. Trace metals as paleoredox and paleoproductivity proxies: an update. Chem. Geol. 232 (1–2), 12–32. https://doi.org/10.1016/j.chemgeo.2006.02.012.
Tribovillard, N., Algeo, T.J., Lyons, T., Riboulleau, A., Bout-Roumazeilles, V., 2008. A possible capture of molybdenum during early diagenesis of dysoxic sediments. Bull. Soc. Geol. Fr. 179 (1), 3–12. https://doi.org/10.2113/gssgfbull.179.1.3.
Tribovillard, N., Riboulleau, A., Lyons, T., Baudin, F., 2004. Enhanced trapping of molybdenum by sulfurized marine organic matter of marine origin in Mesozoic limestones and shales. Chem. Geol. 213 (4), 385–401. https://doi.org/10.1016/j.chemgeo.2004.08.011.
Ulrich, K.-U., Singh, A., Schofield, E.J., Bargar, J.R., Veeramani, H., Sharp, J.O., Bernier-Latmani, R., Giammar, D.E., 2008. Dissolution of biogenic and synthetic UO_2 under varied reducing conditions. Environ. Sci. Technol. 42, 5600–5606. https://doi.org/10.1021/es800647u.
van Helmond, N.A.G.M., Jilbert, T., Slomp, C.P., 2018. Hypoxia in the Holocene Baltic Sea: comparing modern versus past intervals using sedimentary trace metals. Chem. Geol. 493, 478–490. https://doi.org/10.1016/j.chemgeo.2018.06.028.
Vaquer-Sunyer, R., Duarte, C.M., 2008. Thresholds of hypoxia for marine biodiversity. Proc. Natl. Acad. Sci. U. S. A 105 (40), 15452–15457. https://doi.org/10.1073/pnas.0803833105.
Vahtera, E., Conley, D.J., Gustafsson, B.G., Kuosa, H., Pitkänen, H., Savchuk, O.P., Tamminen, T., Viitasalo, M., 2007. Internal ecosystem feedbacks enhance nitrogen-fixing cyanobacteria blooms and complicate management in the Baltic Sea. Ambio 36, 186–194. https://doi.org/10.1579/0044-7447(2007)36[186:iefenc]2.0.co;2.
Veeramani, H., Alessi, D.S., Suvorova, E.I., Lezama-Pacheco, J.S., Stubbs, J.E., Sharp, J. O., Dippon, U., Kappler, A., Bargar, J.R., Bernier-Latmani, R., 2011. Products of abiotic U(VI) reduction by biogenic magnetite and vivianite. Geochem. Cosmochim. Acta 75 (9), 2512–2528. https://doi.org/10.1016/j.gca.2011.02.024.
Virtasalo, J.J., Hämäläinen, J., Kotilainen, A.T., 2014. Toward a standard stratigraphical classification practice for the Baltic Sea sediments: the CUAL approach. Boreas 43 (4), 924–938. https://doi.org/10.1111/bor.12076.
Virtasalo, J.J., Kohonen, T., Vuorinen, I., Huttula, T., 2005. Sea bottom anoxia in the Archipleago Sea, northern Baltic Sea – implications for phosphorus remineralization at the sediment surface. Mar. Geol. 224, 103–122. https://doi.org/10.1016/j.margeo.2005.07.010.

Virtasalo, J.J., Schröder, J.F., Luoma, S., Majaniemi, J., Mursu, J., Scholten, J., 2019. Submarine groundwater discharge site in the First Salpausselkä ice-marginal formation. Solid Earth 10, 405–423. https://doi.org/10.5194/se-10-405-2019.

Vorlicek, T.P., Helz, G.R., Chappaz, A., Vue, P., Vezina, A., Hunter, W., 2018. Molybdenum burial mechanism in sulfidic sediments: iron-sulfide pathway. ACS Earth and Space Chemistry 2, 565–576. https://doi.org/10.1021/acsearthspacechem.8b00016.

Vorlicek, T.P., Kahn, M.D., Kasuya, Y., Helz, G.R., 2004. Capture of molybdenum in pyrite-forming sediments: role of ligand-induced reduction by polysulfides. Geochem. Cosmochim. Acta 68 (3), 547–556. https://doi.org/10.1016/S0016-7037(03)00444-7.

Wagner, M., Chappaz, A., Lyons, T.W., 2017. Molybdenum speciation and burial pathway in weakly sulfidic environments: insights from XAFS. Geochem. Cosmochim. Acta 206, 18–29. https://doi.org/10.1016/j.gca.2017.02.018.

Wan, J., Tokunaga, T.K., Brodie, E., Wang, Z., Zheng, Z., Herman, D., Hazen, T.C., Firestone, M.K., Sutton, S.R., 2005. Reoxidation of bioreduced uranium under reducing conditions. Environ. Sci. Technol. 39, 6162–6169. https://doi.org/10.1021/es048236g.

Wang, Y., Bagnoud, A., Suvorova, E., McGivney, E., Chesaux, L., Phrommavanh, V., Descostes, M., Bernier-Latmani, R., 2014. Geochemical control on uranium(IV) mobility in a mining-impacted wetland. Environ. Sci. Technol. 48, 10062–10070. https://doi.org/10.1021/es501556d.

Wersin, P., Hochella Jr., M.F., Persson, P., Redden, G., Leckie, J.O., Harris, D.W., 1994. Interaction between aqueous uranium (VI) and sulfide minerals: spectroscopic evidence for sorption and reduction. Geochem. Cosmochim. Acta 58 (13), 2829–2843. https://doi.org/10.1016/0016-7037(94)90117-1.

Widerlund, A., Nowell, G.M., Davison, W., Pearson, D.G., 2012. High-resolution measurements of Sulphur isotope variations in sediment pore-waters by lase ablation multicollector inductively coupled plasma mass spectrometry. Chem. Geol. 291, 278–285. https://doi.org/10.1016/j.chemgeo.2011.10.018.

Winterhalter, B., Flodén, T., Ignatius, H., Axberg, S., Niemistö, L., 1981. Geology of the Baltic Sea. In: Voipio, A. (Ed.), The Baltic Sea. Elsevier, Amsterdam, the Netherlands, pp. 1–121.

Xu, N., Christodoulatos, C., Braida, W., 2006. Adsorption of molybdate and tetrathiomolybdate onto pyrite and goethite: effect of pH and competitive anions. Chemosphere 2 (10), 1726–1735. https://doi.org/10.1016/j.chemosphere.2005.06.025.

Zheng, Y., Anderson, R.F., van Geen, A., Fleischer, M.Q., 2002a. Remobilization of authigenic uranium in marine sediments by bioturbation. Geochem. Cosmochim. Acta 66 (10), 1759–1772. https://doi.org/10.1016/S0016-7037(01)00886-9.

Zheng, Y., Anderson, R.F., van Geen, A., Fleischer, M.Q., 2002b. Preservation of particulate non-lithogenic uranium in marine sediments. Geochem. Cosmochim. Acta 66 (17), 3085–3092. https://doi.org/10.1016/S0016-7037(01)00632-9.

Zheng, Y., Anderson, R.F., van Geen, A., Kuwabara, J., 2000. Authigenic molybdenum formation in marine sediments: a link to pore water sulfide in the Santa Barbara Basin. Geochem. Cosmochim. Acta 64 (24), 4165–4178. https://doi.org/10.1016/S0016-7037(00)00495-6.

Zhou, C., Vannela, R., Hyun, S.P., Hayes, K.F., Rittmann, B.E., 2014. Growth of *Desulfovibrio vulgaris* when respiring U(VI) and characterization of biogenic uraninite. Environ. Sci. Technol. 48, 6928–6937. https://doi.org/10.1021/es501404h.